Performance Enhancement of Solar Chimney Power Plant from Geothermal Power Plant Waste Heat

MSc. Thesis

By

Tereche Getnet Tesfa

Thermal and Aerospace Engineering Program

School of Mechanical, Chemical and Materials Engineering

Adama Science and Technology University

Adama, Ethiopia

October 2018

Performance Enhancement of Solar Chimney Power Plant from Geothermal Power Plant Waste Heat

MSc. Thesis

By

Tereche Getnet Tesfa

A Thesis Submitted to Thermal and Aerospace Engineering Program of School of Mechanical, Chemical and Materials Engineering, Adama Science and Technology University in partial fulfillment of the requirement of the degree of Master of Science in Thermal Engineering.

Adviser: Dr. V. Chandraprabu

Co-Advisor: Muzeyin Ahmed

Adama, Ethiopia

October 2018

Declaration

I hereby declare that this MSc. Thesis entitled "**Performance Enhancement of Solar Chimney Power Plant from Geothermal Power Plant Waste Heat**" in partial fulfillment of the requirement of the degree of Master of Science in Thermal Engineering is an authentic record of my own work carried out from September 2017 to September 2018 under supervision of Dr. V. Chandraprabu, Assistant Professor of Thermal Engineering program and Mr. Muzeyin Ahmed, Lecture(MSc.) in Thermal Engineering program, Adama Science and Technology University, Ethiopia.

The matter embedded in this thesis has not been submitted for the award of a degree or diploma in any other university. All relevant resource information used in this paper has been duly acknowledged.

__________________ _________________ _______________

Name Signature Date

This is to certify that the above statement made by the candidate is correct to the best of our knowledge and belief. This has been submitted for examination with our approval.

________________________ _________________ _______________

Advisor Signature Date

________________________ _________________ _______________

Co-Advisor Signature Date

ADAMA SCIENCE AND TECHNOLOGY UNIVERSITY

SCHOOL OF MECHANICAL, CHEMICAL AND MATERIAL ENGINEERING

Thermal and Aerospace Engineering Program

Approval of Board of Examiners

We, the undersigned, members of the Board of Examiners of the final open defense by Tereche Getnet have read and evaluated his thesis entitled " **Performance Enhancement of Solar Chimney Power Plant from Geothermal Power Plant Waste Heat**" and examined the candidate. This is, therefore, to certify that the thesis has been accepted in partial fulfillment of the requirement of the Degree of Master of science in Thermal Engineering.

______________________	_____________	___________
Chairperson	Signature	Date
______________________	_____________	___________
Internal Examiner	Signature	Date
______________________	_____________	___________
External Examiner	Signature	Date

Abstract

A solar chimney power plant (SCPP) sometimes also called "solar chimney" or just "solar tower" is a renewable energy power plant that transforms solar energy into electricity. The SCPP consists of three essential elements; solar collector roof, chimney tower, and wind turbine(s).

Several technologies exist that can convert solar energy into electrical energy. The solar chimney is part of the solar thermal groups of solar conversion technologies. However, due to its greater scale and simplicity, the solar chimney may have an economic efficiency approaching or exceeding that of the other methods, but it has low efficiency of less than 2%. In addition solar chimney power plant (SCPP) dominated by the solar radiation, its discontinuous operation is an unavoidable problem. Solar chimney efficiency and power output have mainly determined by the efficiency of solar collector roof.

In this thesis, the transient thermal and hydrodynamic behavior of working fluid of solar chimney power plant using waste water were investigated to characterize the performance of solar chimney by numerical and theoretical method. Numerical solution technique used to solve a differential equation form of governing equations using finite difference discretization scheme. The result shows, the collector temperature increases by 7 °C, the pressure potential is found 182.82 Pa, the pressure drop on the turbine was 121.88 Pa, and the pressure loss was 60.94 Pa and the power output 123.59 kW. As a result, the collector efficiency increases from 32% to 43.58% and the overall efficiency of plant increases from 0.176% to 0.242%

From the result, it can conclude that the efficiency of solar chimney power plant is improved and the power fluctuation can be controlled by using geothermal wastewater heat.

Key words: solar chimney, pressure potential, solar updraft tower

ACKNOWLEDGEMENT

First, I would like to give an Enormous thanks to the Almighty God for his continual grace and guidance to finish this project, without which this study would not have been possible.

Next, I got to my deepest gratitude to my advisor Dr. V. Chandraprabu who supported me through my graduate studies. With his guidance, generosity, and patience, I was able to expand my horizons as researcher to look forward and analyze critically my results. I am also grateful to Dr. Addisu Bekele PG coordinator, Mr. Samuel G/Mariam program chair of Thermal and Aerospace Engineering and my Co-advisor Muzeyin Ahmed in a ASTU for their kind help on different occasions throughout my study.

To the Aluto Langano power plant manager, Mr. Habtamu Geremew thank you for your respected reception and willingness. I would like to thank my family for supporting me to complete my thesis work. Their encouragement helped me through my journey. It is also my pleasure to thank Adama Science and Technology University to give for me this free scholarship.

Finally yet importantly, I would like to thank ASTU thermal staff members and friends who were always besides me and played a great role in completion of my work.

TABLE OF CONTENTS

List of Figures

List of Tables

Abbreviations

AR	Area ratio
CFD	Computational fluid dynamics
CSCPP	Conventional solar chimney power plant
DA	Divergent angle
DISC	Divergent inlet solar chimney
DOSC	Divergent outlet solar chimney
IEA	International energy association
MSR	Maximum solar radiation
MPG	Maximum power generation
PFCD	Passive flow control devices
PV	Photovoltaic
SCPP	Solar chimney power plant
SCSUTPP	Sloped collector solar updraft tower power plant
SUT	Solar updraft tower
SUTPP	Solar updraft tower power plant
SSCPP	Sloped solar chimney power plant

Acronyms

A	Area (m^2)
c_p	Specific heat at constant pressure (kJ /kg.K)
D	Diameter (m)
Dh	Hydraulic diameter (m)
f	Friction factor
g	Acceleration of gravity (m /s^2)
Gr	Grashoffs number
G_{sc}	Solar constant (W/m^2)
H_{ch}	Height of chimney tower (m)
H_{coll}	Height of collector (m)

$\overline{H}$	Monthly average daily global radiation on horizontal surface (Wh/m^2day)
$\overline{H}_o$	Extraterrestrial global radiation (W/m^2)
H_{eff}	Effective height (m)
h_{con}	Convective heat transfer coefficient ($W/m^2.K$)
h_r	Radiative heat transfer coefficient ($W/m^2.K$)
h_{crf}	Convective heat transfer coefficient from roof to fluid ($W/m^2.K$)
h_{cpf}	Convective heat transfer coefficient from pipe to fluid ($W/m^2.K$)
h_{cgf}	Convective heat transfer coefficient from ground to fluid ($W/m^2.K$)
h_{rrsky}	Radiative heat transfer coefficient from roof to sky ($W/m^2.K$)
h_{rgr}	Radiative heat transfer coefficient from ground to roof ($W/m^2.K$)
h_{rgp}	Radiative heat transfer coefficient from ground to pipe ($W/m^2.K$)
h_{rrpr}	Radiative heat transfer coefficient from pipe to roof ($W/m^2.K$)
I	Incoming solar radiation (W/m^2)
K	Thermal conductivity (W/ m. K)
l_c	Characteristic length (m)
l	Length (m)
$\dot{m}$	mass flow rate (kg/s)
N	Number of days
Nu	Nusselt number
P	Power output (kW)
Pr	Prandtl number
P	Pressure (Pa)
Δp_{pot}	Pressure potential (Pa)
Δp_{loss}	Pressure loss (Pa)
Δp_{tur}	Pressure drop on the turbine (Pa)
Q	Heat flux (kJ/s)
Re	Reynolds number
Ra	Rayleigh number
S	Inclined length of solar collector roof (m)

T	Temperature (K)
U	Velocity (m/s)
X	Power coefficient

Greek letters

N	Kinematic viscosity coefficient (m^2/s)
P	Density (kg/m^3)
Η	Efficiency
μ	Dynamic viscosity (Pa. s)
ε	Emissivity
ϒ	Specific heat ratio
Σ	Steffen Boltzmann constant
Δ	Declination angle
Θ	Incident angle
Φ	Latitude
Β	Collector inclination angle
Α	Absorptivity
Τ	Transmissivity

Subscripts and superscripts

1	Inlet of collector
2	Outlet of collector and inlet of chimney
3	Outlet to turbine
4	Outlet of chimney
A	Ambient air
B	Beam
Ch	Chimney
con	Convection
coll	Collector
D	Diffuse
Eff	Effective
F	Fluid(flowing air in the collector)
Fm	Mean fluid temperature
G	Ground

P	Pipe
R	Roof/Radative
Sut	Solar updraft tower
W	Water/wind

CHAPTER 1
Introduction

1.1. Renewable Energy Technology

Renewable energy is generally defined as energy that comes from resources that are not significantly depleted by their use, such as sunlight , wind, rain , tides , waves and geothermal heat. Renewable energy is gradually replacing conventional fuels in four distinct areas: electricity generation, hot water/space heating, motor fuels, and rural (off-grid) energy services.

Based on REN21 's 2017 report, renewables contributed 19.3% to our energy consumption and 24.5% to our electricity generation in 2015 and 2016 [1] . This energy consumption is divided as 9.1% coming from traditional biomass, 10.2% from modern renewables. Among the modern renewable energies, 3.6% hydroelectricity, 1.6% Electricity from (wind, solar, geothermal, and biomass), 4.2% from (biomass, geothermal and solar heat) and 0.8% biofuels for transport. Renewable energy resources exist over wide geographical areas, in contrast to other energy sources, which are concentrated in a limited number of countries. Rapid deployment of renewable energy and energy efficiency is resulting in significant energy security , climate change mitigation , and economic benefits. In international public opinion surveys there is strong support for promoting renewable sources such as solar power and wind power. By 2022, global renewables electricity generation expected to grow by more than one-third to over 8 000 terawatts per hour, equal to the total consumption of China, India and Germany combined. The share of renewables in power generation will reach 30% in 2022, up from 24% in 2016. Wind and solar together will represent more than 80% of global renewable capacity growth in the next five years [1].

At the national level, at least 30 nations around the world already have renewable energy contributing more than 20 percent of energy supply . National renewable energy markets projected to continue to grow strongly in the coming decade and beyond [1].

1.1.1 Hydropower Plant

Hydroelectricity is the term referring to electricity generated by hydropower ; the production of electrical power through the use of the kinetic energy of falling or flowing water . In 2015 hydropower generated 16.6% of the world's total electricity and 70% of all renewable electricity, which continues the rapid rate of increase experienced between 2003 and 2009. Hydropower is produced in 150 countries, with the Asia-Pacific region generating 32 percent of global hydropower in 2010. China is the largest hydroelectricity producer , with 721 TWh of production in 2010, representing around 17% of domestic electricity use.

Ethiopia’s plentiful hydropower resources are distributed in nine major river basins and their innumerable tributaries is estimated to generate an economically affordable energy of about 260 TWH. Ethiopia’s Hydro potential (45,000 MW) constitutes 20% of the total technically feasible potential in Africa. With this potential Ethiopia usually referred as the powerhouse of Africa. However, Ethiopia has utilized less than 5% of its potential so far .Currently, Access to electricity in Ethiopia is 55% [4].

1.1.2 Wind Energy

Wind energy is the kinetic energy associated with the movement of atmospheric air. Wind turbines convert this kinetic energy to useful form power i.e. electricity. The kinetic energy converted to mechanical energy by using turbines and then to electrical energy by using generators.

Wind power is growing at the rate of 17% annually, with a worldwide installed capacity of 432,883 MW at the end of 2015, and is widely used in Europe , Asia, and the United States. Several countries have achieved relatively high levels of wind power penetration, such as 21% of stationary electricity production in Denmark, 18% in Portugal ,16% in Spain, 14% in Ireland and 9% in Germany in 2010. As of 2011, 83 countries around the world are using wind power on a commercial basis. Continuing strong growth, by 2016 wind generated 3% of global power annually [2].

There are two classification of wind power plant based on axis of rotation namely horizontal axis and vertical axis. It can be used singly or in clusters called wind farms as shown in Figure 1.2 below.

Figure 1. 1 Adama II Wind Farm Project

1.1.3 Tidal

Tidal energy generated by utilizing the natural rise and fall of the coastal tides, onshore or offshore. Onshore, seawater allowed filling an estuary through sluices, which shut at peak high tide. The estuary then drained through turbines, which generate electricity. Offshore, electricity generations by means of tidal flow over horizontal-axis turbines (similar to wind turbines) as well as over aero foil-type generators researched.

1.1.4 Biomass

Biomass is the renewable source derived from the carbonaceous waste of various human and natural activities. It derived from numerous sources, including the byproducts from the timber industry, agricultural crops, raw materials from the forest, major parts of household waste and wood. It does not have carbon dioxide emission to the environment. Biofuels used in solid, gas and liquid form and when burning these fuels, chemical energy converted to thermal energy or heat. Solid biofuels include materials such as wood, straw and different types of organic waste. The possibilities of planting high-energy crops for use as an energy source also explored. Liquid biofuels include fuels like methanol, ethanol and vegetable oils, which derived from biomass to produce a combustible liquid. Biogas produced by the digestion of human and animal waste or by capturing methane gas from municipal landfill sites.

1.1.5 Wave

Wave energy is a renewable source of energy, which based on the conversion of kinetic energy from ocean waves to electric energy. Various shoreline and offshore devices designed and installed worldwide. The shoreline devices include the oscillating water column (OWC), tapered channel (TAPCHAN) and Pendulator.

1.1.6 Solar Energy

Solar energy comes to Earth in the form of radiation, or sunlight, with spectral components mostly in the visible, near infrared, and near ultraviolet. According to well-established measurements, the average power density of solar radiation just outside the atmosphere of the Earth is 1366 W/m^2, widely known as the solar constant. A mere 0.01% of the annual solar energy reaching Earth can satisfy the energy need of the entire world [2]. The incoming radiation can use mainly in two ways. Directly sun radiation is converted to electricity by using PV cells and solar radiation is converted to thermal energy and then to electricity or other applications. Many different concepts explored in an attempt to harness the sun's energy, with the most noteworthy being Central Receiver, Photovoltaic, Parabolic trough collectors and Linear Fresnel reflector.

1.1.7 Geothermal Energy

Geothermal energy derived from the natural heat of the earth .The various types of renewable energies presented in the previous sections are derivatives of solar energy. Deep geothermal energy, on the other hand, is the only major energy source not derived from solar energy. At the time Earth formed from hot gas, the heat and gravitational energy made the core of Earth red-hot. After Earth formed, the radioactive elements continuously supplied energy to keep the core of Earth hot. We can use the steam and hot water produced inside the earth to heat buildings or generates electricity, which extracted by drilling wells to these sources. Since the water replenished by rainfall and the heat continuously produced inside the earth so that geothermal is renewable energy.

Aluto Langano is the first geothermal field in Ethiopia exploited. In this area, eight deep exploration wells (LA-1 to LA-8) drilled from 1981 to 1986 with a maximum depth of 2500 m, reaching temperatures of up to 335 °C [2]. The feasibility studies for this power station were conducted in 1986.The report concluded that the area could support a commercially viable geothermal power station. In May 1998, the first 7.2 MW electric power plants installed in the Aluto Langano field by the Ethiopian Electric Power Corporation and connected to the national power grid. It started by connecting four production wells, LA-3, LA-4, LA-6 and LA-8, and one reinjection well, LA-7 as shown in table 1.1 below. Now a days it is one of the three grid-ready thermal power stations in the country , the other two are the 500 MW Corbetti Caldera Geothermal Power Station and the Tulu Moye Geothermal Power Station , also with capacity of 500 MW. The Aluto Langano geothermal field covers an area of about 8 km^2, capable of generating up to 100 MW electric power[5].

Table 1. 1 Data Summery of Aluto Langano Plant [5]

Wells	**Mass flow rate(kg/s)**	**Pressure(bar)**	**Reservoirs temperature(°C)**	**Turbine Inlet temperature and pressure**
LA-3	10	12.5	315	187.5 °C ,12 bar
LA-6	12.5	13.5	335	
LA-4	26.5	6	235	151.8 °C, 5.4 bar
LA-8	15	8.4	265	

Figure 1. 2 Aluto Langano Geothermal Power Plant

1.2. The Solar Chimney Power Plant

The solar chimney power plants (SCPP) are latest technology that combines solar energy and wind turbines. The main function of the SCPP setup is to convert the solar energy into electrical energy. The SCPP have three main parts; chimney, solar collector and turbine (or turbines). The air heated up inside the solar collector due to solar radiation. Consequently, the air pressure differential generated between inside and outside of system. It causes continuous airflow traveling from the ambience into the chimney through the solar collector. The turbine (or turbines) set at the path of airflow converts the kinetic energy of air into electricity. As proved technique, the solar chimney power plant (SCPP) is representing a simple configuration of the SUPP, but it is not efficient, where it comprises four conversions of energy. Solar radiation converted to thermal energy in the absorbing medium, the thermal energy converted to kinetic energy in the collector passage, the kinetic energy converted to mechanical energy in the wind rotor, and finally, the mechanical energy converted to electrical power through the generator. This series of conversions caused the system efficiency to be as low as less than 2%. The following advantages make the power plant attractive technology for future green energy production with slight drawbacks.

1.2.1. Advantages of Solar Chimney Power Plant

- Solar chimney power plants utilize beam and diffuse solar radiation. Therefore, although reduced, the plant still generates power under cloudy conditions.
- The ground (soil) underneath the collector of a solar chimney power plant acts as a natural energy storage mechanism. This means that, although reduced, the plant continues to generate power at night.
- Construction materials (mainly glass and concrete) for such a plant are relatively inexpensive and readily available.
- The plant operates using simple technology. Except for possibly the turbo-generator, the technology of a solar chimney power plant will not become outdated easily.
- The plant does not require any non-renewable fuels in order to operate and does not produce any emissions. This also means that the plant would never have to deal with escalating fuel costs.
- At suitable plant sites such as desert areas, solar radiation is a very reliable input energy source. Consequently, energy produced by solar chimney power plants will not produce power spikes that may occur with schemes such as wind energy generation.
- The plant has a long operating life (at least 80 to 100 years).
- Solar chimney power plants do not require any cooling water.
- Low maintenance cost.

1.2.2. Disadvantages of Solar Chimney Power Plant

- In order to be economically viable, solar chimney power plants have to build on a very large scale. Due to its size, the initial capital cost of such a plant is high.
- The power output is not constant throughout the day or year. Output during peak energy demand times (early in the morning and early evening) are low while power production is at its peak in times of low electricity demand. Power generation is also much lower in the colder months of the year, when electricity demand is high. Further development may however reduce or even eliminate these disadvantages.

- The construction of the plant requires huge quantities of materials. Such quantities may cause logistical problems regarding the availability and transportation of the materials.
- No structures of similar scale built before.

1.2.3. Comparison with Hydroelectric Power Plants

Solar chimneys are technically very similar to hydroelectric power stations – so far the only successful large-scale renewable energy source: the collector roof is the equivalent of the reservoir, and the chimney of the penstock. Both power generation systems work with pressure-staged turbines, and both achieve low power production costs because of their extremely long life span and low running costs.

The collector roof and reservoir areas required are also comparable in size for the same electrical output. However, the collector roof constructed in arid deserts and removed without any difficulty even if useful (often even populated) land submerged under reservoirs. Solar chimneys work on dry air and can be operated without the corrosion and cavitation typically caused by water. They will soon be just as successful as hydroelectric power stations.

Solar chimneys can convert only a small proportion of the solar heat collected into electricity, and thus have a "poor efficiency level". However, they make up for this disadvantage by their cheap, robust construction and low maintenance costs. Solar chimneys need large collector areas. As economically viable operation of solar electricity production plants confined to regions with high solar radiation, this is not a fundamental disadvantage; as such, regions usually have enormous deserts and unutilized areas. Therefore, "land use" is not a particularly significant factor, although of course deserts are also complex biotopes that have protected.

1.3. Statement of the Problem

Solar energy is one of the renewable energy that covers the world's energy consumption in the future. Solar chimney is the fast growing renewable energy technology that can provides the world's energy consumption. However, the efficiency of the plant is small less than 2%. The circulation of months and variation of ambient conditions limits the continuous supply of energy. Thus this work investigates the improvement of the solar chimney power plant efficiency by using wastewater from geothermal power plant as a heat source.

1.4. Objective of the Study

The general objective of this study is to investigate performance of enhancement of solar chimney power plant using waste heat from geothermal power plant.

The specific objectives of this study are:

- To analyze the transient thermal behavior of collector roof, ground, fluid and geothermal water pipe by using numerical methods.
- To analyze pressure distribution of working fluid in the collector by using numerical methods and estimate the efficiency of solar collector and chimney.
- To estimate optimum dimensional arrangement and power output of plant components.

1.5. Significance of the Study

The significances of the study are:

- Support international agreements and national energy action plans to increase the use of renewable energy due to the growing concerns of pollution. .
- Utilize the rejected heat from geothermal power plant.

1.6. Scope and Limitation

1.6.1. Scope

This study focuses on the theoretical and numerical investigation of transient thermal and hydrodynamic behavior of solar chimney power plant to produce power by utilizing wastewater heat from geothermal power plant that operates at Aluto Langano weather condition.

1.6.2. Limitation

This work is delimited to investigate the transient thermal and hydrodynamic behavior of solar chimney power plant using wastewater heat both numerically and theoretically. The cost analysis of the power plant is not included here. It is expected that the thermo-physical properties of collector roof, solar chimney, ground and geothermal water pipe is a function of temperature, but this study delimited to assume all thermo physical properties are constant.

CHAPTER 2
Literature Review

Solar chimney power plant is the renewable energy in growing technology which can substitute the limited energy resource. The plant have three main parts; working fluid which is air, solar collector and long cylindrical shape called chimney. As the radiation from the sun penetrates solar collector the air beneath it heats and hence the density variation produce updraft through the chimney, which drives the turbo generator. The solar chimney power plant system first proposed in the late 1970s by Schlaich, (1995) and tested with a prototype model in Manzanares, Spain in the early 1980s. They constructed the first prototype in Manzanares, spian and the data collected from this pilot plant were published by Haaf et al, (1983, 1984) in which a brief discussion of the energy balance, design criteria, and cost analysis was presented. This prototype works without fail for seven years that producing 50 kW. However, the performance of the plant is less than 2%. To improve the efficiency of this plant many researchers investigated. Using a detailed thermal analytical model, Bernardes et al, (2003) showed that the height of chimney, the factor of pressure drop at the turbine, the diameter and the optical properties of the collector are the most important parameters for the solar chimney design.

Ayadi et al, (2018) evaluated the performance of SCPP by using different chimney configurations and the numerical simulations showed that the divergent and opposing chimney have greater power generation capacity. Zhou et al, (2017) evaluate the effect of diurnal ambient temperature on the power output of SCPP. The authors found that the increase of diurnal ambient temperature increase the power output of the nighttime and decrease daytime. However, the daily power output is increasing and smooth power output in a small extent. Ming et al, (2017) evaluates the numerical simulation of the effect of ACW on the performance of SCPP which results the performance of plant is increased by novel design of radial partition walls (RPW) for ambient cross wind between 5 and 15 m/s.

Lal et al, (2016) done on the enhancement of plant performance, detail position of components and individual efficiency with optimal range conditions. The turbine installation location decided by the maximum velocity point, which estimated with the help of CFD simulation as to be 0.25–1 m inside the chimney pipe. The effect of chimney height, inlet temperature and the solar radiation was also evaluated and developed the model equation for performance measurements, where producing higher mass flow rate is due to solar radiation is the measure constraint of higher performance. The efficiency of solar collector found to be in the range of 10–19.7%.

Hu et al, (2017) studied the effect of chimney geometry on the performance of SC and reported that divergent chimney greatly increases the performance of the plant but degrades when the AR and DA increases resulted in parabolic shape for power curve. the author's also reported that after normalizing the power output of divergent solar chimney, imposing geometric similarity on the structure of different size will have nearly the same power output. Latter on the authors reported on another work that AR controls the strength of the enhancement effect and DA controls rate of parabolic trend. In another work, Hu et al, (2017) reported that diffuser-type SCs generally have a better power generation performance than the cylindrical SC. The optimal output of the examined DSCs is 13.5 times higher than that of cylindrical SC. The increase in the output from the DISCs ranges from 2 to 10 times while the optimal situation from the DOSCs is only 5 times.

Kumar and Sarkar, (2017) simulate the solar updraft tower and found that the static inlet temperature of chimney is greater than exit static temperature. The simulation shows the difference in static pressure along the tower height and minimum at bottom of tower.

Shirvan et al, (2017) investigated the enhancement of SCPP using sensitivity analysis of critical parameters; collector entrance height, chimney height, chimney diameter and collector inclination angle. They found that the sensitivity of optimal power output to entrance gap and chimney diameter increases with increase in collector entrance height, chimney height and diameter but reduces with increase of collector inclination angle.

Cao et al, (2017) proposed new methods to simplify the complexity of high chimney called solar double chimney power plant. The simulation shows SDCPP have 1.59 times greater than CSCPP and 2.77 times greater than SSCPP. Kassien et al, (2017) investigated the effect of turbine blade quantity, chimney height and collector diameter on the performance of plant. The simulated results show increasing the angular velocity of the turbine decreases the mass flow rate and increases torque and power of turbine. According to this investigation, the maximum mass flow rate occurs in three blades, while the maximum power observed in five bade turbines.

Ayadi et al, (2017) conduct an experiment and computational study the effect of chimney height on the performance of plant. The report shows that chimney height is the main component of plant to determine the power output of solar chimney power plant and an increase of chimney height by 3 m increases 176% the magnitude of velocity. In another work, Ayadi et al, (2018) and AlTaaie et al, (2016) investigated the contribution of collector inclination angle and concluded that negative inclination angle favors greater power output for the plant.

Hassan et al, (2018) conduct a numerical simulation on the effect of chimney diverging angle and collector slope and reported that increasing collector slope below 6° increases the air velocity gradually, but increasing above 6° vortices detected due to uneven distribution of temperature along the collector. likewise ,the effect of chimney diverging angle simulation results shows increasing the power output by 108% by employing 1° diverging angle**.** Choi et al, (2016) develops an analytical model for solar chimney power plants with and without water storage systems. The result shows that solar chimney with water storage has continuous power output and the difference of maximum and minimum power out decreased with regard to depth of water storage.

Mostafa et al, (2018) incorporated a 3-D numerical simulation to investigate the performance of the solar chimney power plant at different weather conditions. Khalil and Sabah, (2018) conducted an experiment on a new design of hybrid solar chimney with PV cells and found that the solar chimney with PV cell collectors without glass cover have greater electrical power output than PV cells with glass covers. However, the kinetic power of the solar chimney increased in a PV cells with glass cover. Fathi et al, (2018) have done on efficiency enhancement of SCPP by use of waste heat from nuclear power plant increases the Manzanares prototype by 150% annually.

Cao et al, (2018) investigated the full year simulation of SCPP and found that the annual accumulated energy generation mainly based on the air temperature rise in the collector and the height of the system. In this work the author's also compares the power generation of CSCPP and SSCPP based on maximum solar radiation (MSR) and maximum power generation(MPG) ,which results the CSCPP generates higher power than SSCPP at MSR angle.

Tayebi and Djezzar, (2016) construct a mathematical model to investigate the effect of ambient temperature and solar radiation on the flow in the collector. The author reports that the temperature and velocity of fluid shows increasing as the radius of collector increases but velocity increases more sharply at chimney inlet. However, the static pressure profile decreases through the collector and drops considerably near the chimney base.

Guo et al, (2016) evaluate the optimal turbine pressure drop ratio and found that with an increase in solar radiation and a decrease in ambient temperature the pressure drop ratio on the turbine increases. In addition, the author reported the superiority of circular collectors over square collectors in the performance of SCPP. Piyush et al, (2016) conduct an experiment to analyze the parameters of SCPP and result show that the increase of mass flow rate favors maximum temperature in larger chimney height and the minimum value of density occurred at the out let of chimney.

Li et al, (2016) analyze the power generation quality and geometric optimization of solar chimney power plant and reported that there is strong relation between power quality factor and chimney height, as well as negative relationship between collector radius and power quality factor. Moreover, there exist the optimal chimney diameter and the optimal collector height to maximize the generation efficiency. The increases of the radius and the height of the solar collector, the decreases of the height and the diameter of the chimney and the appropriate storage layer thickness can improve the power stability of SCPPs.

Ghalamchi et al, (2016) investigate the experimental setup to enhance the performance in different geometric parameters showed that chimney height and diameter are the most influential parameter and have optimum dimensions. Reducing or increasing from this has negative effect on the efficiency of power plant. The author also compared iron plat and aluminum and results aluminum has high heat transfer rate because of higher thermal conductivity and is best for absorber.

Cottam et al, (2018) studied the effect of canopy profile on a solar thermal chimney performance and the study shows the canopy outlet height shown to be an important parameter as it defines the pressure drop in the flow through the collector-to-chimney transition section. Flat canopy can improve power output but pressure losses occur close to the chimney due to restriction of flow. Exponential improve the efficiency but construction and maintenance could be difficult and costly due to access issue. In this study, segmented canopy profile proposed on the best improvement of power output and simpler design constructions**.**

Stojkovski et al, (2016) demonstrates the capability of CFD technique for the analysis of heat transfer and complex aerodynamics problems particularly solar chimney power plant**.** Mehrpooya et al, (2016) evaluated performance of SCPP; a 3D model generated and solved by CFD method. The thermal and dynamic behavior of the fluid flowing through the chimney analyzed.

Ghalamchi et al, (2015) analyzed the temperature distribution and the fluid velocity in solar chimney setup based on the experimental data and concluded. That air inversion phenomenon directly associated with the geometric parameters and the ambient temperature changes. The entrance distance of the collector is the most influential geometric parameter in solar chimney performance.

Guo et al, (2016) analyzed numerically the optimal turbine drop ratio under constant solar radiation. When the turbine pressure drop Increases, the temperature raises increases while the updraft velocity gradually decreases. An increase in the turbine pressure drop means the turbine resulting in a reduction of the updraft velocity extracts more energy. Hence, the heating time of the airflow inside the collector is prolonged and the temperature rise increases. Meanwhile, when the turbine pressure drop remains constant, both the temperature rise and updraft velocity increase significantly with solar radiation.

Later on, Guo et al, (2015) investigate 3D model incorporating radiation model, solar load model and real turbine load. The increase in rotational speed of turbine decrease turbine and collector efficiency, but there is increase in rise in temperature at collector out let and decrease in volume flow rate. This enhances driving force and decrease in discharging in kinetic energy, which leads to increase of system performance. A reasonable assumption should consider evaluating turbine model by fan model. The result also shows zenith angle has effect on collector efficiency and increase the zenith angle from 0°to 30° decreases power output by 17.3% in this study.

Koonsrisuk and Chitsomboon, (2013) proposed a simple method to evaluate the turbine power output for solar chimney systems using dimensional analysis and showed that the optimum ratio between the turbine extraction pressure and the available driving pressure for the proposed plant is approximately 0.84.

Nia and Ghazikhani, (2015) investigated numerically the heat transfer and flow field characteristics using three different passive control shapes that possess three main characteristics, boundary layer agitation, creation of secondary flows and vortices, and enhancing the original flow pattern. Among these, a triangular shape obstacle does not affect the original pattern of the flow from the collector entrance toward the chimney and guides the flow in a more prolific manner. While it is capable of expeditiously creating fluid mixing patterns and thermal boundary layer agitation, hence the greatest velocity and mass flow rate observed. More over 41.2% increment in power production reported in this study.

Ghorbani et al, (2015) investigated numerical simulation for the hybrid system including solar collectors, hot gas flow injection, cooling tower radiators and wind turbine. The power generation enhancement observed in different angles of hybrid tower walls and slopes of collector roof and base ground to illustrate their influence on output power. The investigation shows 0.538% increase in thermal efficiency of the fossil fuel power plant. Patel et al, (2014) and Husain et al, (2014) study the effect of geometric parameters on the performance of SCPP using a computational fluid dynamics (CFD) software ANSYS-CFX. the computation carried on the overall chimney height of 10 m, collector diameter 8m,collector inlet opening ranges from 0.05 m to 0.02 m, collector outlet diameter 0.6 m to 1 m, chimney diverging angle 0° to 3° and the diameter of the chimney 0.25 m to 0.3 m. The result shows that the inlet opening of the collector decreases the power output would increase and in this case, 0.05 m has greater power output. The collector outlet diameter and chimney inlet directly related to power available and has significant influence on the mass flow rate. the researcher also reports divergent chimney have better performance than convergent and cylindrical chimney and in this case 2° diverging angle found to be an optimum.

Chen et al, (2014) perform the thermodynamic analysis of a low temperature waste heat recovery system to investigate the solar chimney tower performance analysis. The system consists of heat exchanger a chimney tower, a turbine and pump. The author reported the system is feasible and can several hundreds of kilowatt power obtained within temperature range of 70 ^{o}C -100 ^{o}C and mass flow rate of 1389 kg/s. The updraft velocity is stable, when the mass flow rate of air and pressure potential is a function of temperature of inflow water, ambient air condition and heat transfer area.

Ali, (2017) proposed a methodology for optimization of solar chimney power plants taking into account the techno-economic parameters. An optimized model was executing for different twelve designs in the range 5–200 MW to cover reinforced concrete chimney, sloped collector, and floating chimney. The resulted payback periods for the floating chimney power plants were the shortest compared to the other studied designs The sensitivity analysis showed that at the same solar radiation and electricity price, the simple payback period for 200 MW with sloped collector design would almost have the double simple payback period for 5 MW with floating chimney design.

Ali, (2013) studied the solar tower power out and its configuration effects on performance. The report shows that collector out let temperature is increasing as both collector diameter and solar radiation increases. The author also obtains the dimensional parameters effect on solar performance as collector diameter, chimney height and chimney diameter in descending order. Hamdan, (2013) analyzed the discrete model chimney and found that the assumption of constant density across the chimney over estimates the harvesting power by the amount of 20%. The report also presents the effect of turbine head on the power output of solar chimney power plant and the maximum power that can produced from the SCPP depends on the selection of the optimum turbine head (or optimum flow rate).

Zhou and Xu, (2016) investigated Variations of pressure potential and inlet air velocity with atmospheric cross flow velocity by changing SUT height and temperature rise. The enlargement effects of pressure potential and SUT inlet air velocity due to the influence of atmospheric cross flow to SUT outlet is found to increase as the SUT height increases, and with lower temperature rise, which is proportional to solar collector area.

Conclusions from the literature

- The efficiency of the power plant is small less than 2% and increasing the dimension of the plant increases the efficiency and power output as shown in table 2.2. Industrial waste heat increase the operation hour and the efficiency of the plant
- The inclination of collector between 1° and 10° increase the performance of the plant
- Chimney height and collector diameter has significance influence on the performance of solar chimney power plant
- Divergent chimney enhances the velocity and airflow rate but has consequence on economic aspect of plant.
- Increasing the collector entrance angle increases the power output of the plant

The present work studies to improve the performance of solar chimney power plant using waste heat from the geothermal power plant. Most of the researchers have done on geometrical parameters to perform the mathematical modeling. The study combines some of the above improvements done on the performance of plant and combines them with new idea of heat source as waste heat in Aluto Langano geothermal power plant. Then, the thesis works using dimensions of plant constructed in Manzanares, Spain height of chimney =194.6 m, diameter of collector=244 m, diameter of chimney=10.16 m. the dimension of the plant are shown in Table 2.1 [6].

Table 2. 1 Typical Dimension of Solar Chimney and their Efficiency in the Literature

Authors	H_{ch} ,m	D_{ch} ,m	D_{coll} ,m	η_{coll} %	η_{ch} %	η_{plant} %	ΔT	uf	CSC PP	Improvement
Shabahang et al, (2015)	12	0.25	5	11	0.04	0.004	20	4	2 W	41.2%increase (PFCD)
Schalachi, (1995)	194.6	10.16	244	32	0.62	0.17	20	9.1	48 kW	74.4 kW(SDCPP)
Gholamalizad, (2016)	247.8	14.79	387.6	35	0.722	0.243	18	4.8	135 kW	175 kW(SSCPP)
Larbi et al, (2010)	200	10	500	50	0.66	0.26	27.5	14.3	140 kW	207.6 kW
Fei chao et al, (2017)	547	54	1100	56	2.6	1.2	13.5	15.3	2.96 MW	4.72 MW(SDCPP)
Zhou et al, (2013)	445	54	1110	56.2	1.45	0.63	25.9	9.1	5 MW	7.13MW(SCSCPP)
Schalachi et al, (1995)	750	84	2200	54.7	2.33	1	31	12.6	30 MW	-
	1500	175	4000	52.6	3.1	1.31	35.7	15.8	100 MW	-

Table 2. 2 Plant Dimension [6].

Parameter	Dimension
Effective chimney height (H_{eff})	194.6 m
Height of chimney(H_{ch})	167.56 m
Chimney diameter (D_{ch})	10.16 m
Collector diameter (D_{coll})	244 m
Collector inlet height	1.85 m
Collector inclination (β)	10°
Collector outlet height(H_{coll})	26.5 m
Number of blade (N)	4
Chimney shape	cylindrical

CHAPTER 3

3.1. Mathematical Model for Collector and Chimney

To determine the mathematical model for SSCPP, the governing equations for the movement of air within the collector and chimney considered separately using the full schematic diagram of the solar chimney power plant in Figure 3.1.

3.1.1. Collector Model

The one-dimensional steady compressible flow in a variable-area passage considered here. It assumed that the solar heat gain totally absorbed by the air under the roof. In the absence of friction and heat loss, the conservation equations in the differential form are as follows:

The continuity equation

$$\frac{\partial \rho}{\partial t} + \frac{d(\rho u A)}{dr} \ldots\ldots\ldots\ldots\ldots\ldots\ldots\ldots\ldots\ldots\ldots\ldots\ldots\ldots\ldots\ldots\ldots \quad (3.1)$$

Momentum equation

$$-\rho u \frac{du}{dr} = \frac{dp}{dr} + \rho g \frac{dh}{dr} + \frac{\partial(\rho u)}{\partial t} \ldots\ldots\ldots\ldots\ldots\ldots\ldots\ldots\ldots\ldots\ldots\ldots\ldots \quad (3.2)$$

Energy equation

$$\frac{\mathrm{dq}}{\mathrm{dr}} = -c_p \frac{dT}{dr} + \frac{\partial\left(c_p \rho T\right)}{\partial t} + u \frac{du}{dr} + g \frac{dh}{dr} \ldots\ldots\ldots\ldots\ldots\ldots\ldots\ldots\ldots\ldots \quad (3.3)$$

State equations

$$\frac{dp}{p} - \frac{d\rho}{\rho} - \frac{dT}{T} = 0 \ldots\ldots\ldots\ldots\ldots\ldots\ldots\ldots\ldots\ldots\ldots\ldots\ldots\ldots \quad (3.4)$$

3.1.2. Chimney Model

The air movement inside a chimney assumed a frictionless adiabatic process. The system of equations for a one-dimensional steady compressible flow in a variable-area chimney is as follows

The continuity equation

$$\frac{\partial\rho}{\partial t}+\frac{d(\rho uA)}{dz}=0 \ldots\ldots\ldots\ldots\ldots\ldots\ldots\ldots\ldots\ldots\ldots\ldots\ldots\ldots\ldots\ldots\ldots\ldots\ldots\ldots\ldots\ldots\ldots\ldots\ldots\ldots\ldots.. (3.5)$$

Momentum equation

$$-\rho u\frac{du}{dz}=\frac{dp}{dz}+\rho g\frac{dh}{dz}+\frac{\partial(\rho u)}{\partial t} \ldots\ldots\ldots\ldots\ldots\ldots\ldots\ldots\ldots\ldots\ldots\ldots\ldots\ldots.. \ldots\ldots\ldots\ldots\ldots\ldots\ldots\ldots\ldots. (3.6)$$

Energy equation:

$$\frac{\mathrm{dq}}{\mathrm{dz}}=-\frac{\mathrm{q}''}{\dot{\mathrm{m}}}\frac{dA}{dz}=c_p\frac{dT}{dz}+\frac{\partial\left(c_p\rho T\right)}{\partial t}+u\frac{du}{dz}+g\frac{dh}{dz} \ldots\ldots\ldots\ldots\ldots\ldots\ldots\ldots\ldots.\ldots.\ldots\ldots\ldots\ldots.\ldots\ldots\ldots. (3.7)$$

State equations:

$$\frac{\mathrm{dp}}{\mathrm{p}}-\frac{\mathrm{d}\rho}{\rho}-\frac{\mathrm{dT}}{\mathrm{T}}=0 \ldots\ldots\ldots\ldots\ldots\ldots\ldots\ldots\ldots\ldots\ldots\ldots\ldots\ldots\ldots\ldots\ldots.\ldots\ldots\ldots\ldots\ldots\ldots\ldots.\ldots\ldots\ldots\ldots\ldots\ldots\ldots.... (3.8)$$

Correspondingly, the following assumptions adopted to simplify the mathematical model:

- Temperature rises in the solar collector is along radial direction [53].
- The collector roof temperature and the ground temperature don't change along the collector radius r, i.e. d/dr for T_{roof} and T_{ground} is zero [43].
- The velocity and temperature gradient on radial direction in the chimney are negligible.
- The analysis is based one-dimensional unsteady flow and the flow in the collector considered as a flow between two parallel plates.
- Boussinesq assumption is valid for the airflow in the chimney [54].
- Ignore the temperature difference between the collector upper and back surface.
- Airflow is under adiabatic condition in the chimney.
- The temperature at some depth below the ground surface is constant.
- There is no radial conduction in the ground surface.

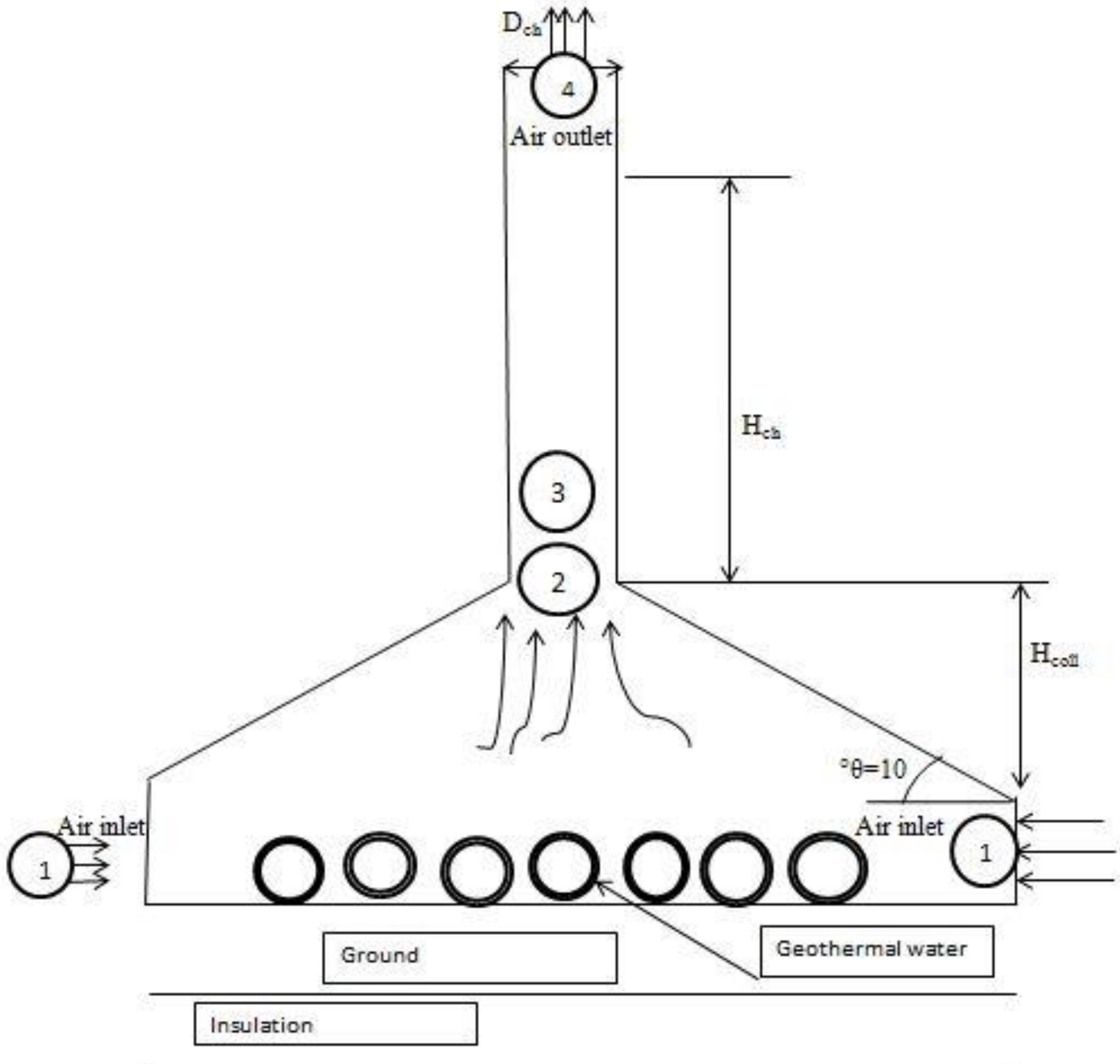

Figure 3. 1 Schematic Diagram of the Combined Geothermal and Solar Chimney Power Plant

3.1. Energy Balance of the Solar Collector Roof

The energy equations are developed based on the plant layout section in figure 3.2 The continuity equation is as follows;

$$m_f = \rho_{f1} A_1 u_{f1} = \rho_{f2} A_2 u_{f2} \ldots \ldots \ldots \ldots \ldots \ldots \ldots \ldots \ldots \ldots \ldots \ldots \ldots \ldots \ldots \ldots \ldots \ldots \ldots \ldots \ldots \ldots \ldots \ldots \ldots \ldots \ldots \ldots .. (3.9)$$

$$where\ A_1 = 2\pi r H_{r1}$$

$$A_2 = \pi r l$$

The energy balance equations are;

For roof:

$$A_{roof}I_{roof} + q_{r,pr} + q_{r,gr} = q_{con,rf} + q_{con,ra} + q_{r,rsky} + c_{pr}\rho_r \frac{dT_r}{dt} 2\pi r_r dr_r z_r \dots\dots\dots\dots (3.10)$$

$$A_{roof} = 2\pi rs \dots\dots\dots 3.11)$$

$$\mathrm{q_{r,pr}} = h_{\mathrm{r,pr}} A_{\mathrm{pipe}}(\mathrm{T_p} - \mathrm{T_r}) \dots\dots\dots (3.12)$$

$$q_{\mathrm{con,rf}} = \mathrm{hc,rf} A_{\mathrm{roof}}(\mathrm{T_r} - \mathrm{T_{fm}}) \dots\dots\dots (3.13)$$

$$\mathrm{q_{con,ra}} = \mathrm{h_{con,ra}} A_{\mathrm{roof}}(\mathrm{T_r} - \mathrm{T_a}) \dots\dots\dots (3.14)$$

$$q_{r,rsky} = h_{r,rsky} A_{roof}(T_r - T_{sky}) \dots\dots\dots ,, (3.15)$$

$$\mathrm{q_{r,gr}} = h_{\mathrm{r,gr}} A_{\mathrm{ground}}(\mathrm{T_g} - \mathrm{T_r}) \dots\dots\dots (3.16)$$

For air

$$\mathrm{mc_p} \frac{dT_{\mathrm{f}}}{dt} = q_{con,rf} + q_{con,pf} + q_{con,gf} - \dot{m} c_p \partial \frac{T_f}{\partial r} dr \dots\dots\dots (3.17)$$

$$q_{con,pf} = h_{con,pf} A_{pipe}(T_p - T_{fm}) \dots\dots\dots (3.18)$$

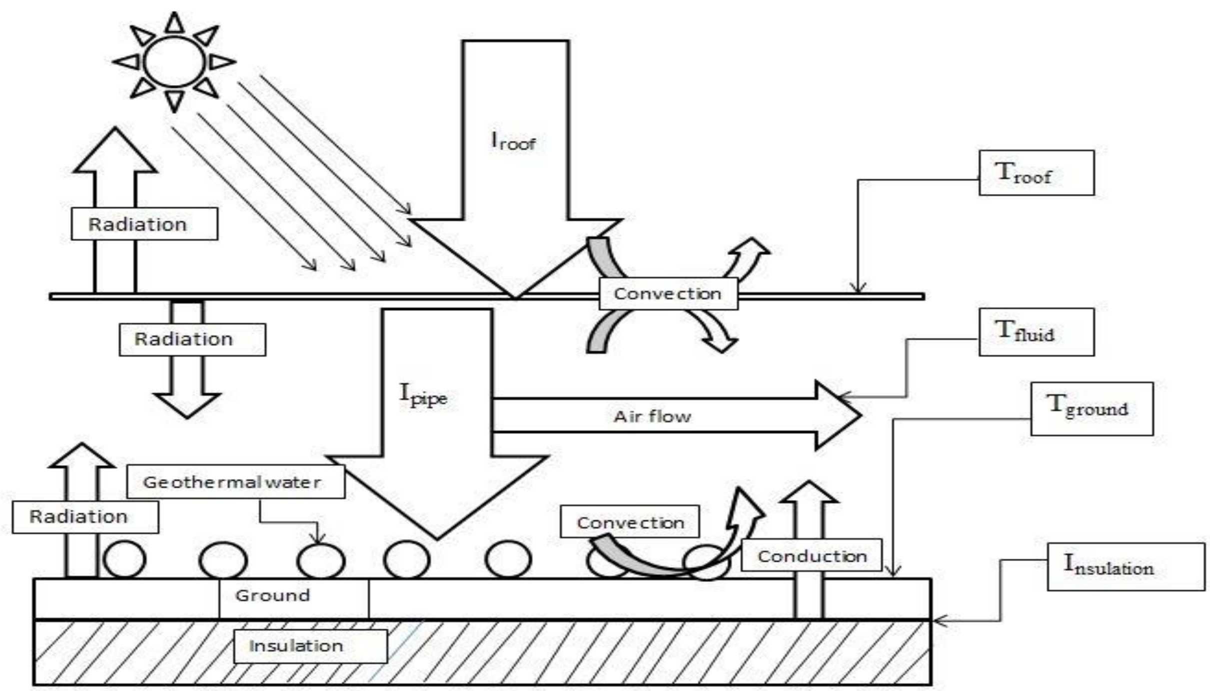

Figure 3. 2 Energy Balance Diagram of plant section

$$q_{con,gf} = h_{con,gf} A_g (T_g - T_{fm}) \dots \quad (3.19)$$

For geothermal pipe

$$A_{\text{pipe}} I_{\text{p}} + q_{r,rp} + q_{r,gp} + \frac{2\pi l_p \, k_p}{\ln(\frac{r2}{r1})}(T_w - T_p) = q_{con,pf} + c_{pp}\rho_p 2\pi r_p \frac{dT_p}{dt} drz_p \dots \quad (3.20)$$

$$q_{r,rp} = h_{\text{r,rp}} A_{\text{pipe}} \left(T_r - T_p\right) \dots \quad (3.21)$$

$$q_{con,pf} = h_{\text{con,pf}} A_{\text{pipe}} \left(T_p - T_{fm}\right) \dots \quad (3.22)$$

$$q_{r,gp} = h_{\text{r,gp}} A_{\text{ground}} \left(T_g - T_p\right) \dots \quad (3.23)$$

For the ground storage

$$A_{ground} I_g + q_{r,rg} + q_{r,pg} - A_{ground} h_{con,gf} \left(T_g - T_{fm}\right) = c_{pg}\rho_g 2\pi r \frac{dT_g}{dt} drdz \dots \quad (3.24)$$

3.2. Estimation of Incident Solar Radiation

The solar radiation incident on the earth's surface depends upon geographical location and a climatic condition of the place, a study of solar radiation under local climatic conditions results good estimation. The total incident radiation is the sum of the beam and diffuses radiation on the horizontal surface and the total radiation on the surfaces that reflect to the tilted surface. The monthly average hourly total radiation on an inclined surface calculated from the knowledge of the monthly average daily total radiation on horizontal surface, $\overline{H}$.

The monthly average of daily total radiation on a tilted surface at a given location, for a particular day, follows the well-established equations [55]. The monthly average extraterrestrial radiation on a surface is calculated by using eq (3.25). Monthly average daily radiation on horizontal surface calculated using eq (3.26) and shown in the figure 3.4.

$$\overline{H}_o = \frac{24*3600*G_{sc}}{\pi}\left(1 + 0.003\cos\frac{360n}{365}\left(\cos\phi\cos\delta\sin\omega_s + \frac{\pi\omega_s}{180}\sin\delta\sin\phi\right)\right) \dots \quad (3.25)$$

The sunrise hour angle calculated as;

$$\omega_s = \cos^{-1}(-\tan\phi \tan\delta)$$

$$\frac{\overline{H}}{\overline{H}_O} = a + b\left(\frac{\overline{n}_s}{\overline{N}_s}\right) \dots \quad (3.26)$$

Where, $\delta = 23.45\sin(360\,\frac{284+n}{365})$

$\overline{H}_o$ In Wh/m²day

$\overline{H}$, Monthly average daily radiation on horizontal surface

$\overline{n}_s$- Monthly average daily hours of bright sunshine

The length of sunshine hours ($\overline{N}_s$) computed from Cooper's formula and shown in the Figure 3.3 below.

$$\overline{N}_s = \left(\frac{2}{15}\right)\omega_s$$

$$a = -0.0110 + 0.235\cos\phi + 0.323\left(\frac{\overline{n}_s}{\overline{N}_s}\right)$$

$$b = 1.449 - 0.533\cos\phi - 0.0.694\left(\frac{\overline{n}_s}{\overline{N}_s}\right)$$

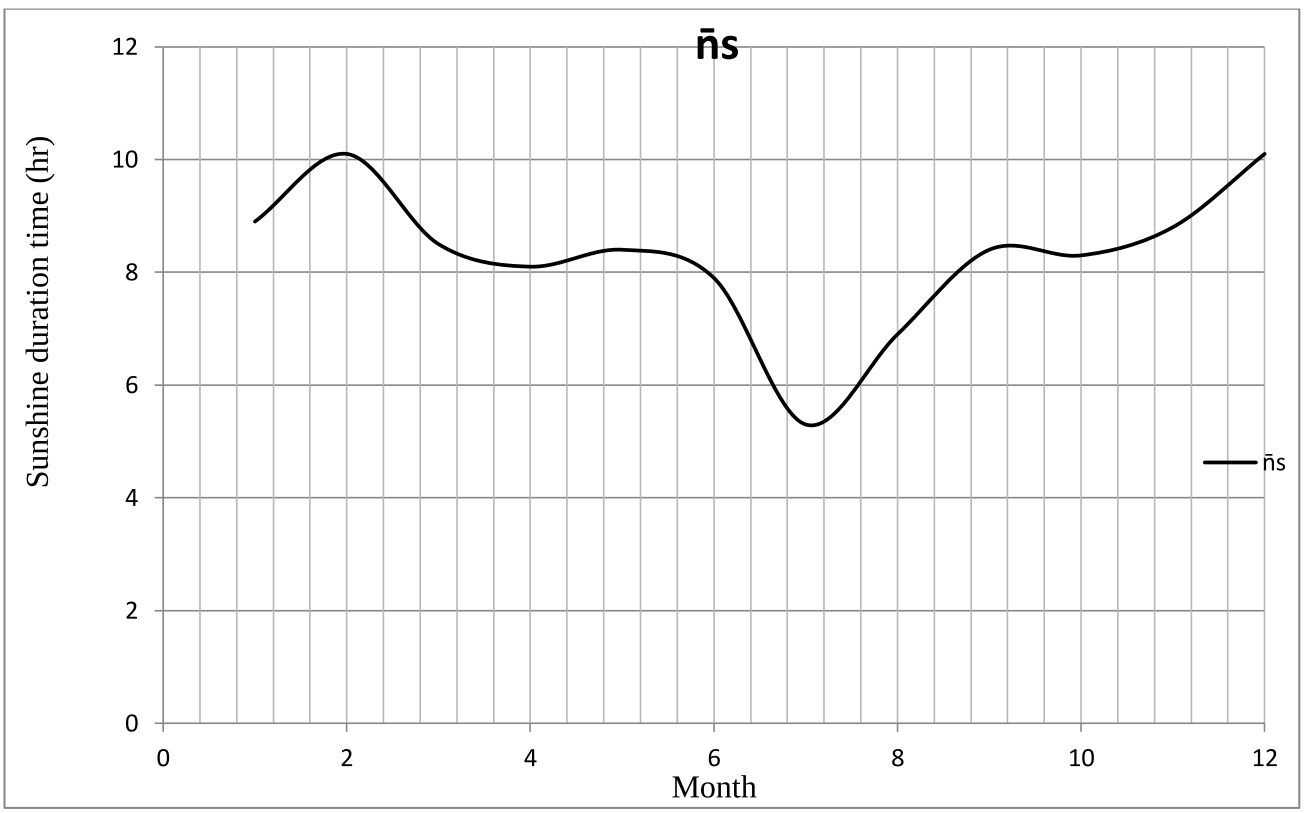

Figure 3. 3 The Length of Sunshine Hour with Representative Day of Month

The monthly average daily diffuse radiation on a horizontal surface can be determined from the monthly average daily global radiation on a horizontal surface and the number of bright sunshine hours.

$$\frac{\bar{H}_d}{\bar{H}} = 0.931 - 0.814\left(\frac{\bar{n}_s}{\bar{N}_s}\right) \quad (3.27)$$

The monthly average hourly global radiation on a horizontal surface calculated from the knowledge of the monthly average daily global radiation on a horizontal surface.

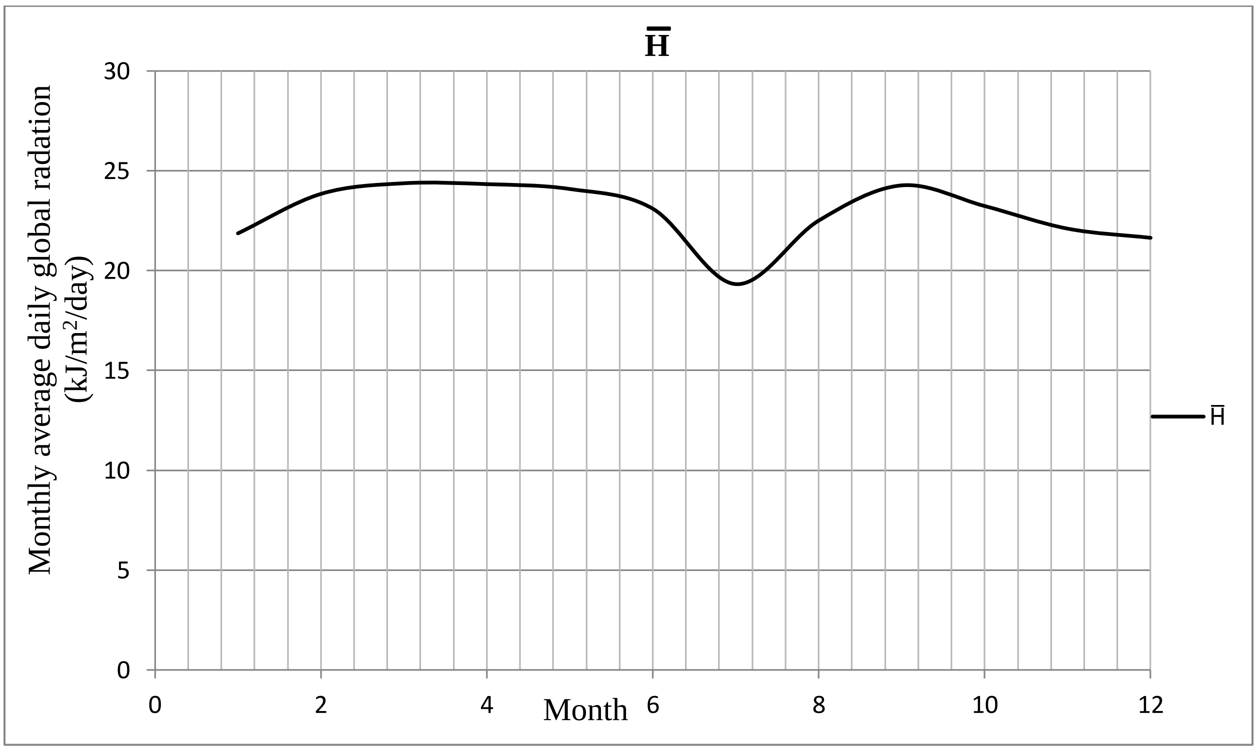

Figure 3. 4 Monthly Average Daily Global Radiation

$$\frac{\bar{I}}{\bar{H}} = \frac{\pi}{24}(a + b\cos\omega)\left(\frac{\cos\omega - \cos\omega_s}{\sin\omega_s - \frac{\pi}{180}\omega\cos\omega_s}\right) \quad (3.28)$$

Where, $a = 0.409 + 0.5016\sin(\omega_s - 60)$

$b = 0.6609 + 0.4767\sin(\omega_s - 60)$

The monthly average hourly diffuse radiation on a horizontal surface calculated from the knowledge of the monthly average daily diffuse radiation on a horizontal surface

$$\frac{\bar{I}_d}{\bar{H}_d} = \frac{\pi}{24}\left(\frac{\cos\omega - \cos\omega_s}{\sin\omega_s - \frac{\pi}{180}\omega\cos\omega_s}\right) \quad (3.29)$$

$$I_T = (\bar{I})R_b + \bar{I}_d\left(\frac{1+cos\beta}{2}\right) + (\bar{I}+\bar{I}_d)\rho\left(\frac{1-cos\beta}{2}\right) \quad (3.30)$$

$$I_{\mathrm{roof}} = \alpha_{\mathrm{roof}} \mathrm{I}_T \quad (3.31)$$

$$I_{\mathrm{p}} = \tau_{roof}\alpha_{pipe}\mathrm{I}_T \quad (3.32)$$

$$I_g = \tau_{pipe}\alpha_{ground}\mathrm{I}_T \quad (3.33)$$

$$R_b = \frac{\cos\theta}{\cos\theta_z} \quad (3.34)$$

Figure 3.5 shows the plot of the Monthly average hourly solar radiation on collector surface with inclined 10° for the whole year. The figure shows the maximum radiation will occur between 10 A.M and 3 P.M for all months.

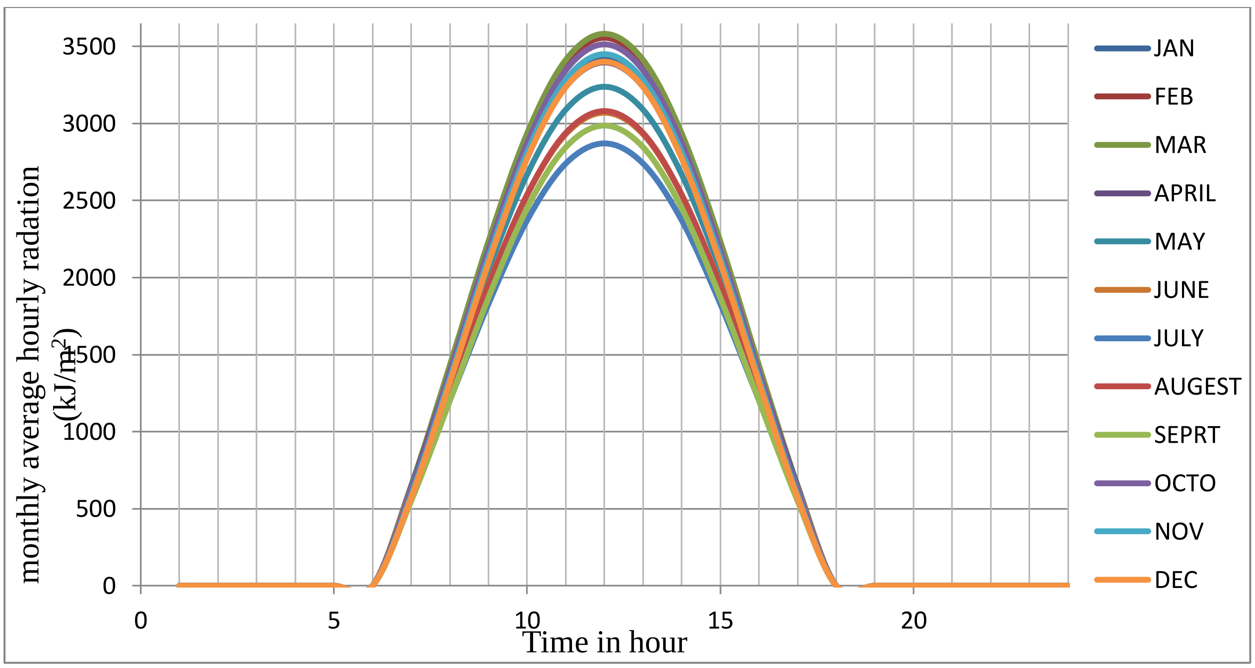

Figure 3. 5 Monthly Average Hourly Solar Radiations With 10° Inclination

3.3. Estimation of Heat Transfer Coefficients

The laws of equations employed for the convective heat transfer coefficients from roof to ambient environment, from roof to the airflow in the collector, and from pipe and absorber to the airflow in the collector can be determined by **Reynolds number** and **Grashofs number** as follows;

$where: Re = \frac{\rho Ulc}{\mu}, Gr = \frac{g\beta(T_s - T_\infty)lc^3}{\nu^2}$

- if Gr/Re^2
  <<1, neglect natural convection,
  >>1, neglecting forced convection,
  =1, natural and forced convection,

$$h_{\text{con,rf}} = \frac{\left(\frac{f}{8}\right)(Re - 1000)Pr}{1 + 12.7\left(\frac{f}{8}\right)^{\frac{1}{2}}(Pr^{\frac{2}{3}} - 1}\left(\frac{k}{d_h}\right) \ldots\ldots\ldots\ldots\ldots\ldots\ldots\ldots (3.35)$$

$$h_{con,ra} = 3.87 + 0.0022\left(\frac{u_w C_p}{Pr^{\frac{2}{3}}}\right) \ldots\ldots\ldots\ldots\ldots\ldots\ldots\ldots (3.36)$$

$$\text{Where, Ra} = \frac{(gcos\theta)\beta(T_s - T_\infty)lc^3}{\nu^2}Pr$$

The general equation for external forced cross flow on cylinders is [53];

$$\frac{h_{con,pf}D}{k} = FNu = CRe^m Pr^n \ldots\ldots\ldots\ldots\ldots\ldots\ldots\ldots (3.37)$$

Where F=0.7, n=1/3 and the other C and m determined experimentally as shown in table 3.1 below.

Table 3. 1 Empirical Correlations for the Average Nusselt Number for Forced Convection Over Circular in Cross Flow

Cross section	**Range of Re**	**C**	**M**
cylinder 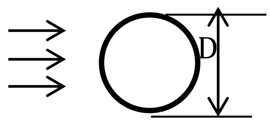	0.4-4	0.989	0.330
	4-40	0.911	0.385
	40-4000	0.683	0.466
	4000-40,000	0.193	0.618
	40,000-400,000	0.027	0.805

$$\frac{h_{con,gf} lc}{k} = Nu_l = \frac{0.3387 Pr^{1/3} Rel^{0.5}}{[1 + (0.0468/Pr)^{2/3}]^{1/4}} \ldots \ldots (3.38)$$

The fluid properties evaluated at the film temperature$\mathrm{T_f} = \frac{(\mathrm{T_{fm}} + \mathrm{T_s})}{2}$, which is the average of the mean fluid air and surface temperatures.

The radiative heat transfer coefficient between the pipe and collector roof, ground and collector roof, pipe, ground, and from the collector roof to the sky are, respectively:

$$h_{\mathrm{r,pr}} = \frac{\sigma(\mathrm{Tp}^2 + \mathrm{Tr}^2)(\mathrm{Tp} + \mathrm{Tr})}{(1/\varepsilon\mathrm{p} + 1/\varepsilon\mathrm{r} - 1)} \ldots \ldots (3.39)$$

$$h_{\mathrm{r,gr}} = \frac{\sigma(\mathrm{Tg}^2 + \mathrm{Tr}^2)(\mathrm{Tg} + \mathrm{Tr})}{(1/\varepsilon\mathrm{g} + 1/\varepsilon\mathrm{r} - 1)} \ldots \ldots (340)$$

$$h_{\mathrm{r,gp}} = \frac{\sigma(\mathrm{Tg}^2 + \mathrm{Tp}^2)(\mathrm{Tg} + \mathrm{Tp})}{\left(\frac{1}{\varepsilon\mathrm{p}} + \frac{1}{\varepsilon\mathrm{g}} - 1\right)} \ldots \ldots (3.41)$$

$$\mathrm{h_{r,rsky}} = \sigma\varepsilon_{\mathrm{r}}\left(\mathrm{T_r}^2 + \mathrm{T_{sky}}^2\right)\left(\mathrm{T_r} + \mathrm{T_{sky}}\right) \ldots \ldots (3.42)$$

3.4. Energy Balance Equations

The discretized energy balance equations carried based on Figure 3.2 as follows;

For roof:

$$A_{roof}I_{roof} + q_{r,pr} + q_{r,gr} = q_{con,rf} + q_{con,ra} + q_{r,rsky} + c_{pr}\rho_r \frac{dT_r}{dt} 2\pi r_r dr_r z_r$$

$$\begin{aligned} A_{roof}I_{roof} + A_{pipe}h_{\mathrm{r,pr}}\left(\mathrm{T_p}^t - \mathrm{T_r}^t\right) + A_{ground}h_{\mathrm{r,gr}}\left(\mathrm{T_g}^t - \mathrm{T_r}^t\right) \\ = \mathrm{hc,rf}A_{\mathrm{roof}}\left(\mathrm{T_r}^t - \mathrm{T_{fm}}^t\right) + \mathrm{h_{con,ra}}A_{\mathrm{roof}}\left(\mathrm{T_r}^t - \mathrm{T_a}^t\right) \\ + h_{r,rsky}A_{roof}\left(T_r^{\ t} - T_{sky}^{\ t}\right) + c_{pr}\rho_r \frac{T_r^{\ t+\Delta t} - T_r^{\ t}}{\Delta t} 2\pi r_r dr_r z_r \end{aligned}$$

$$\begin{aligned} T_r^{\ t+\Delta t} = T_r^{\ t}\Bigg(1 - \frac{\Delta t}{c_{pr}\rho_r 2\pi r_r dr_r z_r}(A_{roof}\mathrm{h_{con,ra}} + A_{roof}\mathrm{h_{con}},\mathrm{rf} + A_{pipe}h_{\mathrm{r,pr}} + A_{ground}h_{\mathrm{r,gr}} \\ + A_{roof}h_{r,rsky})\Bigg) + \frac{\Delta t}{c_{pr}\rho_r 2\pi r_r dr_r z_r}(A_{roof}I_{roof} + A_{pipe}h_{\mathrm{r,pr}}\mathrm{T_p}^t \\ + A_{ground}h_{\mathrm{r,gr}}\mathrm{T_g}^t + A_{roof}\mathrm{h_{con,rf}}\mathrm{T_{fm}}^t + A_{roof}\mathrm{h_{con,ra}}\mathrm{T_a}^t \\ + A_{roof}h_{r,rsky}T_{sky}^{\ t}) \ldots.\ldots.\ldots.\ldots.(3.43) \end{aligned}$$

For flowing air:

$$\dot{\mathrm{m}}\mathrm{c_p}\frac{dT_{\mathrm{f}}}{dt} = q_{con,rf} + q_{con,pf} + q_{con,gf} - \dot{m}c_p\frac{(T_{f,j+1}^{\ t} - T_{f,j}^{\ t})}{dr}$$

$$\begin{aligned} \mathrm{mc_p}\frac{T_{\mathrm{f,j+1}}^{\ t+\Delta t} - T_{\mathrm{f,j+1}}^{\ t}}{\Delta t} \\ = \mathrm{h_{con,rf}}A_{\mathrm{roof}}\left(\mathrm{T_r}^t - \mathrm{T_{fm}}^t\right) + h_{con,pf}A_{pipe}(T_p^{\ t} - \mathrm{T_{fm}}^t) + h_{con,gf}A_{ground}(T_g^{\ t} \\ - \mathrm{T_{fm}}^t) - \dot{m}c_p\frac{(T_{f,j+1}^{\ t} - T_{f,j+1}^{\ t})}{\Delta r} \end{aligned}$$

$$\begin{aligned} T_{\mathrm{f,j+1}}^{\ t+\Delta t} = T_{\mathrm{f,j+1}}^{\ t} + \frac{\Delta t}{mc_p}(\mathrm{h_{con,rf}}A_{\mathrm{roof}}\left(\mathrm{T_r}^t - \mathrm{T_{fm}}^t\right) + h_{con,pf}A_{pipe}(T_p^{\ t} - \mathrm{T_{fm}}^t) \\ + h_{con,gf}A_{ground}(T_g^{\ t} - \mathrm{T_{fm}}^t) - \dot{m}c_p\frac{(T_{f,j+1}^{\ t} - T_{f,j}^{\ t})}{\Delta r}) \end{aligned}$$

$$T_{\mathrm{f,j+1}}{}^{t+\Delta t} = T_{\mathrm{f,j+1}}{}^{t}\left(1-\frac{1}{\Delta r}\right)+\frac{\Delta t}{mc_p}(A_{\mathrm{roof}}\mathrm{h}_{\mathrm{con,rf}}\mathrm{T_r}{}^{t} - A_{\mathrm{roof}}\mathrm{h}_{\mathrm{con,rf}}\mathrm{T_{fm}}{}^{t} + A_{pipe}h_{con,pf}T_p{}^{t} - A_{pipe}h_{con,pf}\mathrm{T_{fm}}{}^{t} + A_{ground}h_{con,gf}T_g{}^{t} - A_{ground}h_{con,gf}\mathrm{T_{fm}}{}^{t} - \dot{m}c_p\frac{T_{f,j}{}^{t}}{\Delta r}) \ldots\ldots\ldots\ldots(3.44)$$

$$\mathrm{T_{fm}}{}^{t} = \frac{T_{\mathrm{f,j+1}}{}^{t} + T_{\mathrm{f,j}}{}^{t}}{2} = \frac{T_{\mathrm{f\,exit}}{}^{t} + T_{\mathrm{f\,inlet}}{}^{t}}{2}$$

For geothermal water pipe:

$$A_{\mathrm{pipe}}I_{\mathrm{p}} + q_{r,rp} + q_{r,gp} + kA_{pipe}\frac{(T_w - T_p)}{dz} = q_{con,pf} + c_{pp}\rho_p 2\pi r_p\frac{dT_p}{dt}l_p dz_p$$

$$A_{\mathrm{pipe}}I_{\mathrm{p}} + A_{\mathrm{roof}}h_{\mathrm{r,rp}}(T_r{}^{t} - T_p{}^{t}) + A_{\mathrm{ground}}h_{\mathrm{r,gp}}(T_g{}^{t} - T_p{}^{t}) + kA_{pipe}\frac{(T_{wm} - T_p{}^{t})}{\Delta z} = A_{pipe}h_{con,pf}(T_p{}^{t} - \mathrm{T_{fm}}{}^{t}) + c_{pp}\rho_p 2\pi r_p\frac{(T_p{}^{t} - \mathrm{T_p}{}^{t+\Delta t})}{\Delta t}l_p dz_p$$

$$\mathrm{T_p}{}^{t+\Delta t} = T_p{}^{t}\left(1-\frac{\Delta t}{c_{pp}\rho_p 2\pi r_p l_p \Delta z_p}\left(A_{\mathrm{roof}}h_{\mathrm{r,rp}} + A_{\mathrm{ground}}h_{\mathrm{r,gp}} + \frac{kA_{pipe}}{\Delta z} + A_{pipe}h_{con,pf}\right)\right) + \frac{\Delta t}{c_{pp}\rho_p 2\pi r_p l_p \Delta z_p}(A_{\mathrm{pipe}}I_{\mathrm{p}} + A_{\mathrm{roof}}h_{\mathrm{r,rp}}T_r{}^{t} + A_{\mathrm{ground}}h_{\mathrm{r,gp}}T_g{}^{t} + \frac{kA_{pipe}}{\Delta z}T_{wm} + A_{pipe}h_{con,pf}\mathrm{T_{fm}}{}^{t}) \ldots\ldots\ldots\ldots (3.45)$$

For the ground heat storage:

$$A_{ground}I_g + q_{r,rg} + q_{r,pg} - q_{con,gf} = c_{pg}\rho_g 2\pi r\frac{dT_{ab}}{dt}drdz$$

$$A_{ground}I_g + h_{\mathrm{r,rg}}A_{\mathrm{roof}}(T_r{}^{t} - T_g{}^{t}) + h_{\mathrm{r,pg}}A_{\mathrm{pipe}}(T_p{}^{t} - T_g{}^{t}) - h_{con,abf}A_{ground}(T_g{}^{t} - \mathrm{T_{fm}}{}^{t}) = c_{pg}\rho_g 2\pi r\frac{T_g{}^{t+\Delta t} - T_g{}^{t}}{\Delta t}dr\Delta z_g$$

$$T_g{}^{t+\Delta t} = T_g{}^t\left(1 - \frac{\Delta t}{c_{pg}\rho_g 2\pi r dr \Delta z_g}\left(h_{\mathrm{r,rg}}A_{\mathrm{roof}} + h_{\mathrm{r,pg}}A_{\mathrm{pipe}} + h_{con,gf}A_{ground}\right)\right)$$

$$+\frac{\Delta t}{c_{pg}\rho_g 2\pi r dr \Delta z_g}\left(h_{\mathrm{r,rg}}A_{\mathrm{roof}}T_r{}^t + h_{\mathrm{r,pg}}A_{\mathrm{pipe}}T_p{}^t + h_{con,gf}A_{ground}\mathrm{T_{fm}}{}^t + A_{ground}I_g\right) \ldots \ldots (3.46)$$

The above discretized equations are solved through iterative MATLAB code (APPENDIX: A1) using the diagrams shown below in Figure 3.6 which results the annual temperature variation of collector roof, ground storage, geothermal water pipe and the flowing fluid air in the collector. The results of the MATLAB code plotted in Figure 4.1,4.2 and 4.3

3.5. Pressure Potential Caused by Sloped Solar Collector and Chimney

The chimney converts the thermal energy produced by the solar collector into kinetic energy. The rising of temperature creates the density difference in the collector that works as the driving force for fluid air. By taking the air as an object, the whole pressure potential converts to the dynamic pressure of airflow. In the assumptions of this compressible flow model, air follows the ideal gas law, and the loss through the SUT wall is negligible. A thermal model based on energy balance developed to predict the performance of the SUT described under different conditions.

The pressure potential of the SUTPP used to drive the current in the plant from the collector inlet to the SUT outlet. It will produce the maximum flow when no any turbine installed and the pressure losses are not considered. The pressure potential of the SUTPP can also be equal to the dynamic pressure at the collector outlet or the SUT inlet under no load conditions by neglecting the pressure losses when air current flows through the plant.

$$\Delta P_{poten} = \frac{1}{2}\rho_3 u_3{}^3 \ldots \ldots \ldots \ldots \ldots \ldots \ldots \ldots \ldots \ldots \ldots \ldots \ldots \ldots (3.47)$$

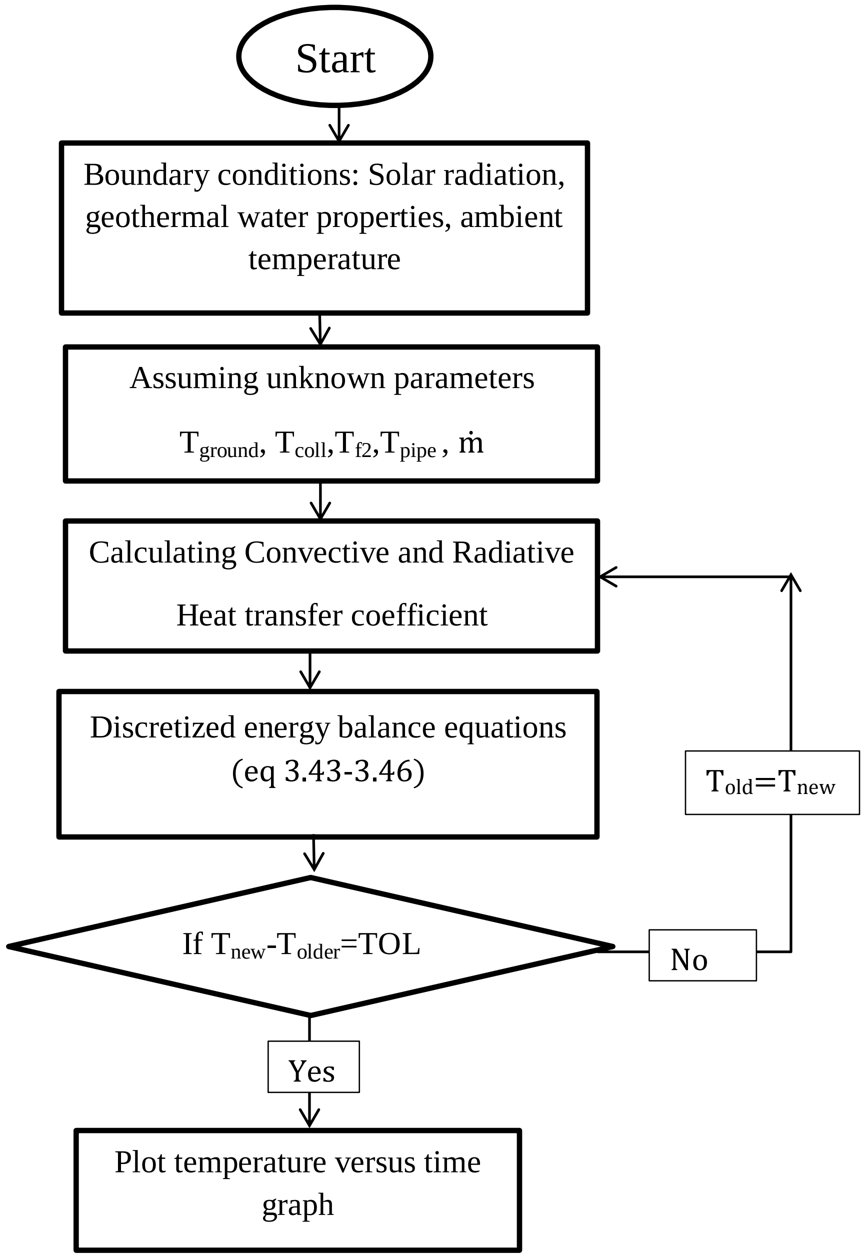

Figure 3. 6 The Flow Chart Procedure of MATLAB Code Developed

The pressure potential of the SUTPP was considered by Koonsrisuk and Chitsomboon, (2013) to be equal to the difference of the static pressures at the collector inlet (point 1) and outlet (point 2) equivalently at the SUT inlet (point 3) under no load conditions, that is ,$(p_1 - p_3)$. The momentum equation without considering the shear stress items for the sloped collector can express as;

$$-\rho u \frac{du}{dr} = \frac{dp}{dr} + \rho g \frac{dh}{dr} \ldots \qquad (3.48)$$

After integration of Eq. (3.48) can written as;

$$\int_1^3 \rho u du = \frac{1}{2}\int_1^3 \rho du^2 = p_1 - p_3 - g\int_1^3 \rho dh \ldots \qquad (3.49)$$

As the indoor air rises from the sloped collector inlet to outlet, the indoor air current should accelerate, and its gravitational potential energy increases, but the static pressure gradually decreases. Gravitational force takes a significant effect on the movement of the air current up the sloped collector.

In order to remove the integral signs in Eq. (3.49) to obtain an expression containing no integral for the SCSUTPP pressure potential, the mean density of the air inside the sloped collector substituted into Eq. (3.47) can rewritten as:

$$\frac{1}{2}\bar{\rho}({u_3}^3 - {u_1}^3) = p_1 - p_3 - g\bar{\rho}H_{coll} \ldots \qquad (3.50)$$

The density of the indoor dry air does not change linearly but decreases exponentially with heights from the inlet (point 1) to the outlet (point two, equivalently the SUT inlet, point three, under no load conditions) of the sloped solar collector. However, the mean density of indoor air for the actual exponential decrease seems to be just slightly larger than the mean density of indoor air for the linear variation. For the sake of simplicity of model, the latter used as $\bar{\rho}$, this can give by:

$$\bar{\rho} = \frac{\rho_1 + \rho_3}{2} \ldots \qquad (3.51)$$

In addition, the expression Eq. (3.50) of the SCSUTPP pressure potential Δp_{poten} can further write as;

$$\Delta p_{pot} = p_{\infty 1} - p_3 - \frac{\rho_{\infty 1} + \rho_3}{2} gH_{coll} \ldots \qquad (3.52)$$

At a random position, the vertical height h above the collector inlet (point 1) can expressed as a function of r and the inclination slope β:

$$h = H_{coll} - r sin\beta \qquad (3.53)$$

The effective SUT height H_{eff} for the SCSUTPP defined to be equal to the sum of the vertical height of sloped collector, H_{coll}, and the SUT height, H_{sut}.

$$H_{eff=}H_{coll} + H_{chimney} \qquad (3.54)$$

The heat losses across the wall and frictional losses are negligible compared with the pressure potential p_{pot}. Therefore, the dry air assumed to experience an isentropic change in state and can describe by:

$$\frac{P}{\rho^{\gamma}} = constant \qquad (3.55)$$

$$\rho = \frac{P}{RT} \qquad (3.56)$$

$$\frac{p_1}{p_2} = \left(\frac{T_1}{T_2}\right)^{\frac{\gamma}{\gamma-1}} \qquad (3.57)$$

$$\frac{\rho_1}{\rho_2} = \left(\frac{T_1}{T_2}\right)^{\frac{1}{\gamma-1}} \qquad (3.58)$$

With the specific gas constant of dry air (R) is equal to $287\,J/kg.K$. Inside the SUT the temperature will changed according to the dry adiabatic lapse rate equal to $0.00975\ K/m$.

$$T = T_o + \frac{g}{R}\frac{1-\gamma}{\gamma}h \qquad (3.59)$$

The static temperature of dry ambient air at a height this expressed as:

$$\frac{T_{\infty}}{T_{\infty 0}} = 1 - \frac{gh}{c_p T_{\infty 0}} \qquad (3.60)$$

Where, $T_{\infty 0}$ is being the temperature of the ambient air at the ground level.

The pressure gradient in a gravity field expressed as

$$\frac{dp}{dz} = -\rho g \quad (3.61)$$

After substitution of Eq. (3.57) into Eq. (3.60) we get

$$p_3 = p_4\left(1 - \frac{gH_{sut}}{c_pT_3}\right)^{\frac{-\gamma}{\gamma-1}} \quad (3.62)$$

$$p_3 = p_{\infty1}\left(\frac{1 - \frac{gH_{eff}}{c_pT_{\infty1}}}{1 - \frac{gH_{sut}}{c_pT_3}}\right)^{\frac{\gamma}{\gamma-1}} \quad (3.63)$$

$$\frac{T_4}{T_3} = 1 - \frac{gH_{sut}}{c_pT3} \quad (3.64)$$

$$\frac{T_\infty}{T_{\infty1}} = 1 - \frac{gh}{c_pT_{\infty1}} \quad (3.65)$$

$$\frac{p_\infty}{p_{\infty1}} = \left(1 - \frac{gh}{c_pT_{\infty1}}\right)^{\frac{\gamma}{\gamma-1}} \quad (3.66)$$

And the standard pressure $p_{\infty4}$ of dry static atmosphere expressed as:

$$p_{static,\infty4} = p_{static,\infty3}\left(1 - \frac{gH}{c_pT_{\infty3}}\right)^{\frac{\gamma}{\gamma-1}} \quad (3.67)$$

The static pressure $p_{\infty4}$ of dry ambient air at the outlet height can express as;

$$p_{\infty4} = p_{static,\infty4} - \frac{1}{2}\rho_{cross}u_{w\,cross}{}^2 \quad (3.68)$$

$$\rho_{cross} = \frac{P_{\infty4}}{RT_{\infty4}} \quad (3.69)$$

$$p_{\infty4} = p_{static,\infty4}\frac{2RT_{\infty4}}{2RT_{\infty4} + u_{w\,cross}{}^2} \quad (3.670)$$

According to Pretorius and Kroger, (2006) the difference of the static pressure at the SUT outlet and the ambient pressure at the same height in windy conditions can express as:

$$p_4 - p_{\infty 4} = c_{po}\frac{1}{2}\rho_{cross}{u_{w\,cross}}^2 \dots\dots\dots\dots\dots\dots\dots\dots\dots\dots\dots\dots\dots\dots\dots\dots\dots\dots\dots\dots\dots\dots\dots\dots(3.71)$$

Where C_{po} is the pressure coefficient at the outlet of SUT. C_{po} may be represented by:

$$C_{po} = -0.405 + 1.07\left(\frac{u_{\infty 4}}{u_4}\right)^{-1} + 1.8\log_{10}\left(\frac{u_{\infty 4}}{2.7v_4}\right)\left(\frac{u_{\infty 4}}{u_4}\right)^{-2} \dots\dots\dots\dots\dots\dots\dots\dots\dots\dots\dots\dots\dots(3.72)$$

$$p_4 = p_{\infty 4} + (c_{po} - 1)\frac{1}{2}\rho_{cross}{u_{w\,cross}}^2 \dots\dots\dots\dots\dots\dots\dots\dots\dots\dots\dots\dots\dots\dots\dots\dots\dots\dots\dots\dots\dots(3.73)$$

During relatively quiet (no significant ambient winds) periods,$(c_{po}1)\frac{1}{2}\rho_{cross}{u_{w\,cross}}^2 = 0$

$$\Delta p_{pot} = p_{\infty 1}\left(1 - \left(\frac{1 - \frac{gH_{eff}}{c_pT\infty_3}}{1 - \frac{gH_{sut}}{c_pT_3}}\right)^{\frac{-\gamma}{\gamma-1}}\right) - \frac{gH_{coll}p_{\infty 1}}{2RT_{\infty 1}}\left(1 + \frac{T_{\infty 1}}{T_3}\left(\frac{1 - \frac{gH_{eff}}{c_pT\infty_3}}{1 - \frac{gH_{sut}}{c_pT_3}}\right)^{\frac{-\gamma}{\gamma-1}}\right)\dots\dots(3.74)$$

The pressure potential converted to dynamic pressure calculated as:

$$\Delta p_{total} = \Delta p_{pot} - \Delta p_{loss} \dots\dots\dots\dots\dots\dots\dots\dots\dots\dots\dots\dots\dots\dots\dots\dots\dots\dots\dots\dots\dots\dots\dots\dots\dots\dots(3.75)$$

The energy conversion efficiency of the SUT defined as the proportion of the fluid power of the air current at the SUT inlet to the heat gains of the heated air current obtained from the solar collector. It can also define as the conversion of heat into kinetic energy, which is practically independent of the rise of air temperature in the collector; it is essentially determined by the outside temperature T_o at ground level and the height of the chimney H_{ch} [6].

$$\eta_{ch} = \frac{\frac{1}{2}\dot{m}_f{u_f}^2}{\dot{m}_fCp(T_{f2} - T_{f1})} = \frac{gH_{ch}}{c_pT_0} \dots\dots\dots\dots\dots\dots\dots\dots\dots\dots\dots\dots\dots\dots\dots\dots\dots\dots\dots\dots\dots\dots\dots(3.76)$$

The efficiency of collector roof is the ratio of useful energy transferred to the fluid air to the incoming solar radiation intercepted by the roof and the heat generation from the geothermal power plant waste heat.

$$\eta_{coll} = \frac{Q_{usefull}}{I_T A_{coll} + Q_{geo}} = \frac{m_f c_{pf}\left(T_{f2} - T_{f1}\right) + 0.5 * m_f ({u_2}^2 - {u_1}^2)}{I_T A_{coll} + m_w c_{pw} (T_{w2} - T_{w1})} \dots\dots\dots\dots\dots\dots\dots\dots \quad (3.77)$$

The above mathematical equations are solved iteratively using flow charts in figure 3.7. The MATLAB code is developed to solve these iterative equations as shown in Appendix: 3.

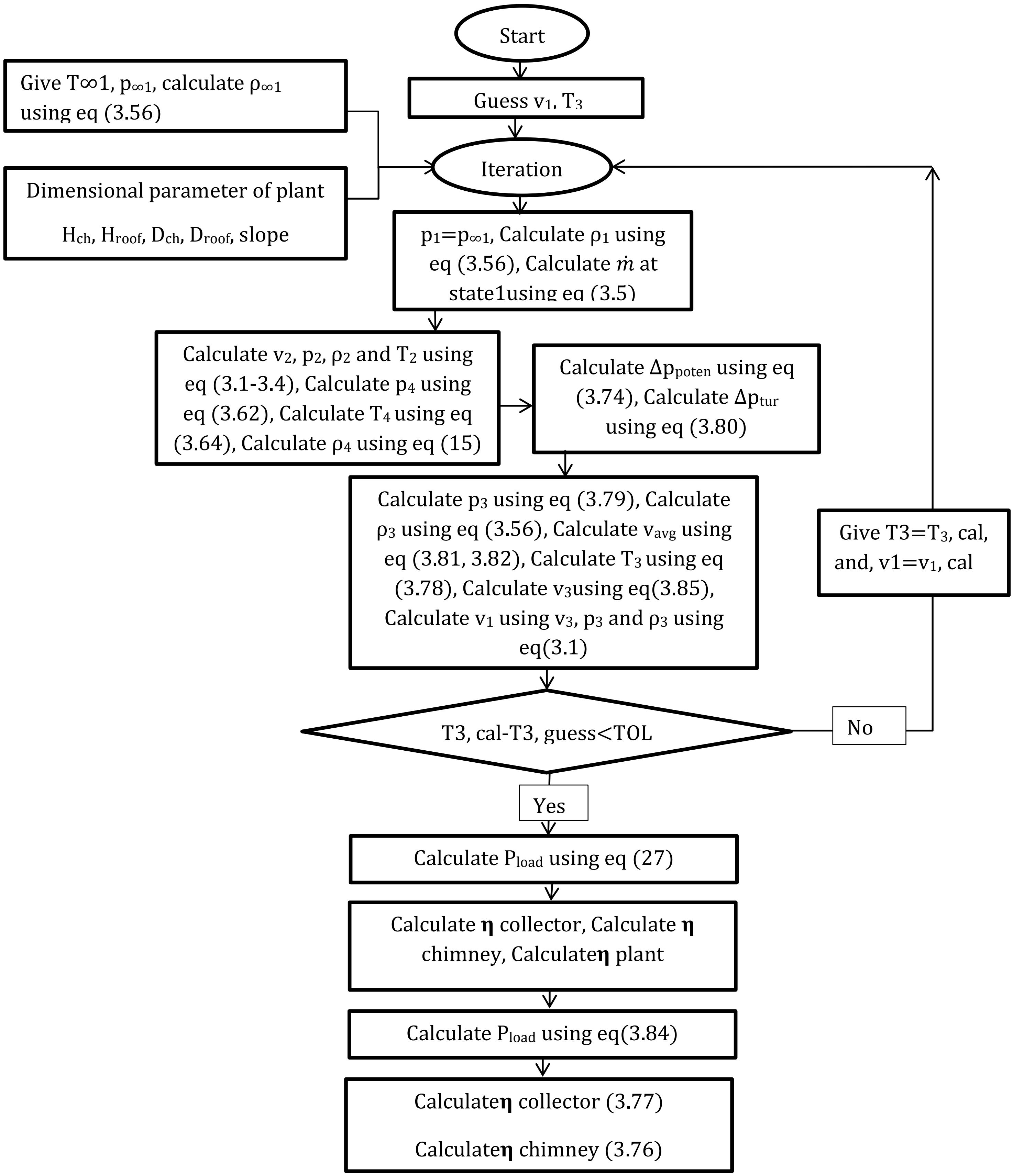

Figure 3. 7 Flowchart of MATLAB Code

3.6. Thermodynamic Analysis of Solar Chimney power plant

The energy conversion processes related to SUTPP can be demonstrated with a temperature-entropy diagram of air standard cycle analysis without considering system losses as shown in Figure 3.8 [62].

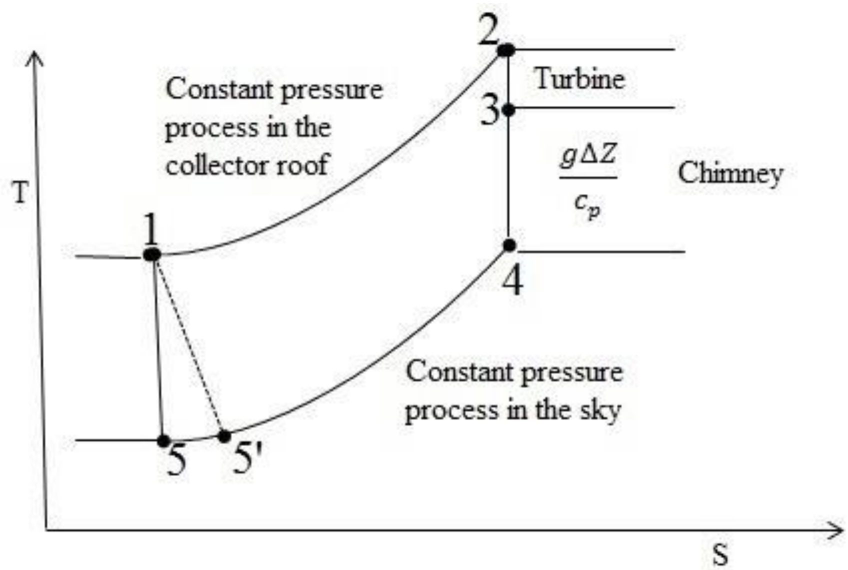

Figure 3. 8 The Diagram of Brayton Cycle Model of Solar Chimney

In the figure, the collector inlet area is assumed large enough, resulting in a small velocity of airflow at the collector inlet. Process 1-2 occurring in the collector denotes that the air entering through the collector inlet from the surroundings heated by solar radiation, its temperature and entropy increase, and the indoor air motion accelerated, while the total pressure kept constant inside the collector. Process 2-3 denotes that the air blows through the turbine into the SUT when the temperature and static pressure decrease slightly. This is entropic process. Process 3-4 denotes that the air behind the turbine flows through the SUT when the temperature decreases mainly due to the negative work done by the gravitational force. This is also an isentropic process. Process 4-5 denotes that the energy including kinetic energy and heat of airflow released into the atmosphere.

In an ideal gas turbine cycle where there are no irreversible processes all the power could be extracted as the gas expands from $p_3$to p_4 to obtain the shaft power m*c_p(T_3-T_4). In the case of the solar chimney, the power required to lift the air up the chimney must be taken into account. The total power available is,

$$P_{available} = \dot{m}c_p(T_2 - T_4) \ldots \ldots \ldots \ldots \ldots \ldots \ldots \ldots \ldots \ldots \ldots \ldots \ldots (3.78)$$

The power required to lift the air up the chimney,

$$P_{lift} = \dot{m}g\Delta z \ldots \ldots \ldots \ldots \ldots \ldots \ldots \ldots \ldots \ldots \ldots \ldots \ldots (3.79)$$

The cycle pressure ratio is defined as:

$$r = \frac{p_1}{p_5} = \frac{p_2}{p_4} \ldots \ldots \ldots \ldots \ldots \ldots \ldots \ldots \ldots \ldots \ldots \ldots \ldots (3.80)$$

And the compression temperature ratio is given by:

$$c = \frac{T_1}{T_5} = \frac{T_2}{T_4} \ldots \ldots \ldots \ldots \ldots \ldots \ldots \ldots \ldots \ldots \ldots \ldots \ldots (3.81)$$

$$c = r^{\frac{(\gamma-1)}{\gamma}} \ldots \ldots \ldots \ldots \ldots \ldots \ldots \ldots \ldots \ldots \ldots \ldots \ldots (3.82)$$

The efficiency is the turbine output power divided by the solar energy transferred to the air moving through the collector.

$$\eta = \frac{shapt\ poweroutput}{thermalpower\ in}$$

The solar energy and geothermal energy transferred to air is:

$$\Delta P_{23} = \dot{m}c_p(T_2 - T_1) \ldots \ldots \ldots \ldots \ldots \ldots \ldots \ldots \ldots \ldots \ldots \ldots \ldots (3.83)$$

The shaft power output is

$$P_{shaft} = \dot{m}c_p(T_2 - T_4) - \dot{m}c_p(T_1 - T_5) \dots\dots\dots\dots\dots\dots\dots\dots\dots\dots\dots\dots\dots\dots\dots\dots\dots\dots\dots\dots\dots\dots\dots. (3.84)$$

$$\eta = \frac{\dot{m}c_p(T_2 - T_4) - \dot{m}c_p(T_1 - T_5)}{\dot{m}c_p(T_2 - T_1)} \dots\dots\dots\dots\dots\dots\dots\dots\dots\dots\dots\dots\dots\dots\dots\dots\dots\dots\dots\dots\dots\dots. (3.85)$$

$$= \frac{(T_2 - T_4) - (T_1 - T_5)}{(T_2 - T_1)}$$

$$= 1 - \frac{(T_4 - T_5)}{(T_2 - T_1)}$$

$$\eta = 1 - \frac{T_5\left(\frac{T_4}{T_5} - 1\right)}{T_1\left(\frac{T_2}{T_1} - 1\right)} \dots\dots\dots\dots\dots\dots\dots\dots\dots\dots\dots\dots\dots\dots\dots\dots\dots\dots\dots\dots\dots\dots\dots\dots\dots\dots\dots (3.86)$$

$$\eta = 1 - \frac{1}{r^{\frac{(\gamma-1)}{\gamma}}} \dots\dots\dots\dots\dots\dots\dots\dots\dots\dots\dots\dots\dots\dots\dots\dots\dots\dots\dots\dots\dots\dots\dots\dots\dots\dots. (3.87)$$

From the above it can be seen that the efficiency is only dependent on the pressure ratio and not on the temperature ratio. In gas turbines the flow variables are often normalized to the inlet condition T_5. The specific power is a function of the cycle temperature ratio t_{52} where $\Delta T_{12}$is the temperature rise in the combustor and $T_1$is the compressor exit temperature. The cycle temperature ratio is defined as:

$$t_{52} = \frac{T_2}{T_5} = \frac{T_1 + \Delta T_{52}}{T_5} \dots\dots\dots\dots\dots\dots\dots\dots\dots\dots\dots\dots\dots\dots\dots\dots\dots\dots\dots\dots\dots\dots\dots\dots.. (3.88)$$

The specific power is normalized with $T_{5,}$

$$P_5 = \frac{P_{shaft}}{\dot{m}c_pT_5} = t_{52}\left(1 - \frac{1}{c}\right) - (c - 1) \dots\dots\dots\dots\dots\dots\dots\dots\dots\dots\dots\dots\dots\dots\dots\dots\dots\dots\dots. (3.89)$$

$$P_5 = (c - 1)\left[\frac{t_{52}}{c} - 1\right] \dots\dots\dots\dots\dots\dots\dots\dots\dots\dots\dots\dots\dots\dots\dots\dots\dots\dots\dots\dots\dots\dots\dots\dots (3.90)$$

For solar chimney

$$c_p(T_1 - T_5) = g\Delta z \quad (3.91)$$

$$\eta = \frac{g\Delta z}{c_p T_1} \quad (3.92)$$

$$P_1 = \frac{P}{\dot{m}c_p T_1} = \frac{\dot{m}c_p(T_2 - T_4) - \dot{m}c_p(T_1 - T_5)}{\dot{m}c_p T_1} \quad (3.93)$$

$$= (\frac{t_{52}}{c} - 1)(1 - \frac{1}{c})$$

$$\frac{t_{52}}{c} = \left(1 + \frac{\Delta T_{12}}{T_1}\right)$$

$$P_1 = \left(\frac{g\Delta z}{c_p T_1}\right)\left(\frac{\Delta T_{12}}{T_1}\right) \quad (3.94)$$

$$P_2 = \frac{P}{\dot{m}c_p T_2} = \frac{\dot{m}c_p(T_2 - T_4) - \dot{m}c_p(T_1 - T_5)}{\dot{m}c_p T_2} \quad (3.95)$$

$$= \left(1 - \frac{1}{c}\right)\left(1 - \frac{c}{t_{52}}\right)$$

$$P_2 = \left(\frac{g\Delta z}{c_p T_1}\right)\left(\frac{\Delta T_{12}}{T_1 + \Delta T_{12}}\right) \quad (3.96)$$

The power from the turbine normalized to T_2 is:

$$P_3 = \frac{\dot{m}c_p(T_2 - T_3)}{\dot{m}c_p T_2} = 1 - \frac{T_3}{T_2} \quad (3.97)$$

The turbine temperature ratio is

$$\frac{T_3}{T_2} = 1 - \left(\frac{g\Delta z}{c_p T_1}\right)\left(\frac{\Delta T_{12}}{T_1 + \Delta T_{12}}\right) \quad (3.98)$$

Once the temperature ratio across the turbine has been found, the ideal gas relationship is used to find the pressure ratio and from this the pressure drop is as follows,

$$\frac{p_3}{p_2} = (\frac{T_3}{T_2})^{\frac{(\gamma-1)}{\gamma}} \dots\dots\dots\dots\dots\dots\dots\dots\dots\dots\dots\dots\dots\dots\dots\dots\dots\dots\dots\dots\dots\dots\dots\dots\dots\dots\dots\dots\dots\dots\dots\dots\dots (3.99)$$

Then the turbine pressure drop is given by;

$$\Delta p_{tur} = p_1 \left[1 - \left[1 - \left(\frac{g\Delta z}{c_p T_1} \right) \left(\frac{\Delta T_{12}}{T_1 + \Delta T_{12}} \right) \right]^{\frac{(\gamma-1)}{\gamma}} \right] \dots\dots\dots\dots\dots\dots\dots\dots\dots\dots\dots\dots\dots\dots\dots\dots (3.100)$$

$$\dot{m} = \frac{P_{required}}{P_1 c_p T_1} \dots\dots\dots\dots\dots\dots\dots\dots\dots\dots\dots\dots\dots\dots\dots\dots\dots\dots\dots\dots\dots\dots\dots\dots\dots\dots\dots\dots\dots\dots\dots\dots\dots (3.101)$$

3.7. Mathematical Modeling of Turbine and Generator

The heat flow produced by the collector converted into kinetic energy (convection current) and potential energy (pressure drop at the turbine) through the chimney. Thus, the temperature rise of the air in the collector causes the density difference that work as a driving force. The lighter column of air in the chimney is connected with the surrounding atmosphere at the base (inside the collector) and at the top of the chimney, and thus acquires lift. Between chimney base and the surroundings, a pressure difference Δp_{pot} produced. When turbines installed between the collector outlet (point 2) and the turbine outlet (point 3) of the system, the temperature and static pressure at (point 3) given by:

$$T3 = T2 - \frac{\Delta P_{tur} A_{sut} u_{avg}}{c_p \dot{m}} \dots\dots\dots\dots\dots\dots\dots\dots\dots\dots\dots\dots\dots\dots\dots\dots\dots\dots\dots\dots\dots\dots\dots\dots\dots\dots\dots (3.102)$$

$$p_3 = p_2 - p_{tur,i} - \Delta p_{tur} \dots\dots\dots\dots\dots\dots\dots\dots\dots\dots\dots\dots\dots\dots\dots\dots\dots\dots\dots\dots\dots\dots\dots\dots\dots\dots\dots\dots (3.103)$$

$$\Delta p_{turb} = x \Delta p_{poten} \dots\dots\dots\dots\dots\dots\dots\dots\dots\dots\dots\dots\dots\dots\dots\dots\dots\dots\dots\dots\dots\dots\dots\dots\dots\dots\dots\dots\dots\dots (3.104)$$

$$u_{avg} = \frac{\dot{m}}{A_{sut} \rho_{avg}} \dots\dots\dots\dots\dots\dots\dots\dots\dots\dots\dots\dots\dots\dots\dots\dots\dots\dots\dots\dots\dots\dots\dots\dots\dots\dots\dots\dots\dots (3.105)$$

$$\rho_{avg} = \frac{p_3 + p_2}{R(T_2 + T_3)} \quad (3.106)$$

$$\Delta p_{loss} = \Delta p_{pot} - \Delta p_{tur} \quad (3.107)$$

$$P_{load} = \eta_{tg} \Delta p_{tur} A_{sut} u_{avg} \quad (3.108)$$

$$\Delta p_{loss} = \Delta p_1 + p_{acc} + p_{br} + p_f + p_4 \quad (3.109)$$

Where, $p_1 = \varepsilon_1 \frac{1}{2} \rho_1 {u_1}^2$

$$p_{acc} = \varepsilon_{acc} \tfrac{1}{2} \rho_3 {u_3}^2$$

$$p_{br} = \varepsilon_{br} \tfrac{1}{2} \rho_3 {u_3}^2$$

$$p_f = f \tfrac{H_{sut}}{D_{sut}} \tfrac{1}{2} \rho_3 {u_3}^2$$

$$p_4 = \varepsilon_4 \frac{1}{2} \rho_4 {u_4}^2$$

The inlet loss, the vertical accelerating axial airflow, the inside wall friction, the internal bracing wheel drag forces, and the outlet loss all contribute to a pressure drop over the height of the SUT. The pressure loss coefficients recommended as the wall friction factors $f = 0.008428$, the vertical accelerating axial airflow pressure loss coefficients $\varepsilon_{acc} = 0.27$, and the inlet loss coefficient $\varepsilon_1 = 0.25$ and the same value was assumed for the loss coefficient ε_{br} due to the internal SUT bracing by cables or rods.

$$\varepsilon_4 = -0.28 {Fr_D}^{-1} + 0.04 {Fr_D}^{-1.5}$$

$$Fr_D = (\frac{\dot{m}}{A_1})^2 [\rho_4 (\rho_{\infty 4} - \rho_4) g D]$$

Where, $Fr_D is$ the densimetric Froude number.

The total efficiency of the power plant is depending on the component efficiency of plant. It is defined as by what amount the power output extracted from the input energy.

$$\eta_{total} = \frac{P_{load}}{A_{coll} I_T} = \eta_{tg}\eta_{coll}\eta_{ch} \qquad (3.110)$$

Selecting a 6-pole 3-phase synchronous speed generator, the rotor speed at 50 Hz is 1500 rpm. The tip speed ratio for a specified diameter rotor given by;

$$\lambda = \frac{\Omega R}{u} \qquad (3.111)$$

$$\mu = \frac{r}{R} \qquad (3.112)$$

For ease of manufacture, due to its flat high-pressure side, selecting NACA0012 blade design with lift coefficient (C_l), angle of attack (α) and the flow induction factor (a) for optimum operation at constant speed. The expression given by:

$$\lambda C_1 N c 2\pi r = \frac{\left(\frac{8}{9}\right)}{\sqrt{\left(\left(1-\frac{1}{3}\right)^2 + \lambda^2\mu^2(1+(\frac{2}{9}(\lambda^2\mu^2))^2\right)}} \qquad (3.113)$$

$$\tan\phi = \frac{1-\frac{1}{3}}{\left(1+\left(\frac{2}{(3\lambda\mu)^2}\right)\right)} \qquad (3.114)$$

$$\beta = \phi - \alpha \qquad (3.115)$$

Where, ϕ is the local inflow angle, α is the angle of attack, β is the blade twist angle, Ω rotor speed in rpm, λ is tip speed ratio and N is the number of blade [58].

3.8. Mathematical Modeling of Geothermal Water Pipe

The geothermal wastewater introduced at the outlet of fluid air in the collector roof and discharged at the inlet of fluid air. The length of the geothermal water pipe can determine by log mean temperature difference of cross flow between air and geothermal water.

$$\Delta T_{ln} = \frac{\Delta T1 - \Delta T2}{\ln(\Delta T1/\Delta T2)} \qquad (3.116)$$

$$U A_s \Delta T_{ln} = \dot{m}_w c p_w (T_{w1} - T_{w2}) \ldots\ldots\ldots\ldots\ldots\ldots\ldots\ldots\ldots (3.117)$$

$$A_s = \frac{m_w c p_w (T_{w1} - T_{w2})}{U \Delta T_{ln}} \ldots\ldots\ldots\ldots\ldots\ldots\ldots\ldots\ldots (3.118)$$

$$As = \pi D_p L_p \ldots\ldots\ldots\ldots\ldots\ldots\ldots\ldots\ldots (3.119)$$

The pipe is oriented in circular way as shown in Figure 3.9 in which the inlet of geothermal water is at the entry of fluid air and exit is at the outlet of collector. The pipe circulates 40 rounds with 3 m spacing between each round.

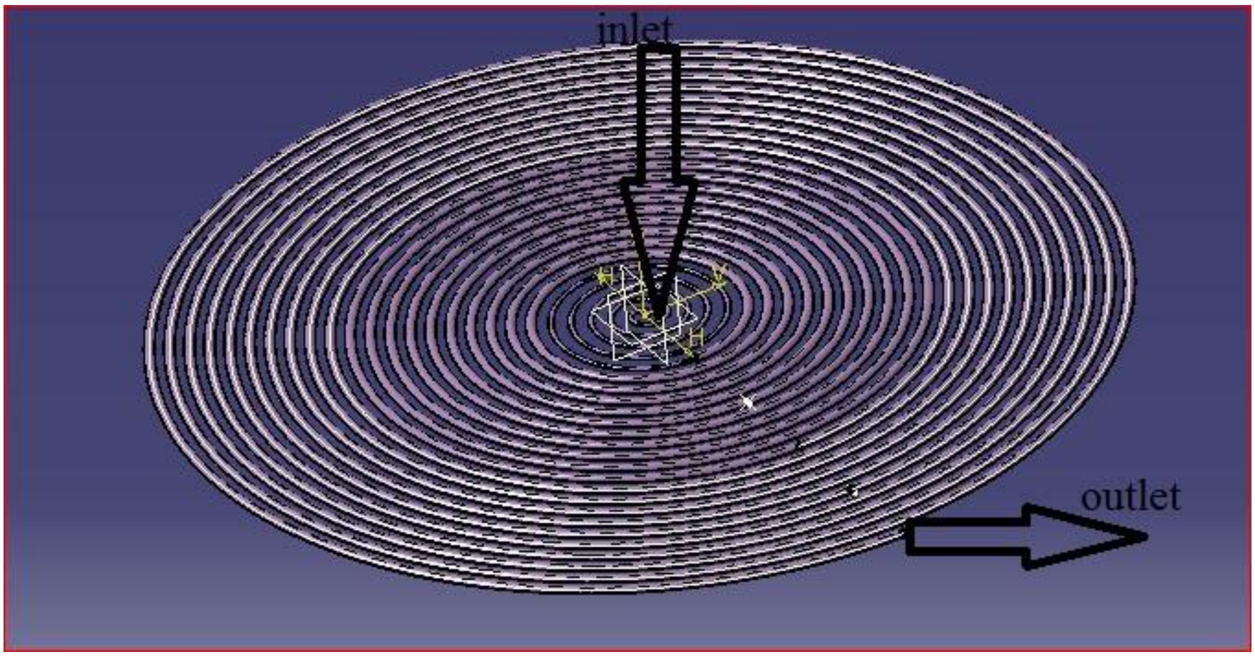

Figure 3. 9 Geothermal Water Pipe Arrangements

CHAPTER 4

4.1. Simulation Results and Discussion

The initial condition of the plant on Aluto Langano weather condition are tabulated in Table 4.1 by using this initial conditions numerical solutions are solved. The simulation result of the Figure 3.7 are tabulated in Table 4.2.

Table 4. 1 Assumed and Initial Condition

Initial condition		**Assumed condition**	
Parameter	Value	Parameter	Assumed value
Ambient temperature, Ta	18 °C	Roof temperature, T_r	50 °C
Inlet fluid temperature,T_{f1}	18 °C	Outlet fluid temperature,T_{f2}	45 °C
Inlet geothermal water temperature,T_{w1}	90 °C	Ground temperature, Tg	60 °C
Outlet geothermal water temperature,T_{w2}	Ta+20 °C	Geothermal water pipe temperature, Tp	55°C
Mass flow rate of geothermal water, $\dot{m}_w$	62.5 kg/s	Mass flow rate of fluid air,$\dot{m}_f$	1525 kg/s
Specific capacity of water	4190 J/kg.K		

Table 4. 2 The Output Parameter at Each Section of Plant

State	**Pressure (Pa)**	**Temperature (°K)**	**Density (kg/m³**	**Velocity (m/s)**
state1	90000	293	1.0703	3
state2	89901	318	0.98505	15.801
state3	89783	319	0.98067	7.909
state4	99044	317.1	1.0883	14.936
	Δp_{poten}=182.82 Pa	$\Delta p_{turb=}$121.88 Pa	$\Delta p_{loss=}$ 60.94 Pa	ΔP_{load}=123.59 kW

In Figure 4.1, four Figures plotted together which shows annual temperature variation of roof, ground, fluid airflow and pipe. The highest fluid air temperature observed in the month of November, December and January; which is approximately 323.3°K. The minimum temperature observed in august. The temperature profile of all figures is similar in shape as shown, which shows the ground temperature is the maximum observed temperature because of the ground is acts as absorber in the system. It absorbs the incoming solar radiation and emits back to the collector roof and fluid air in the collector.

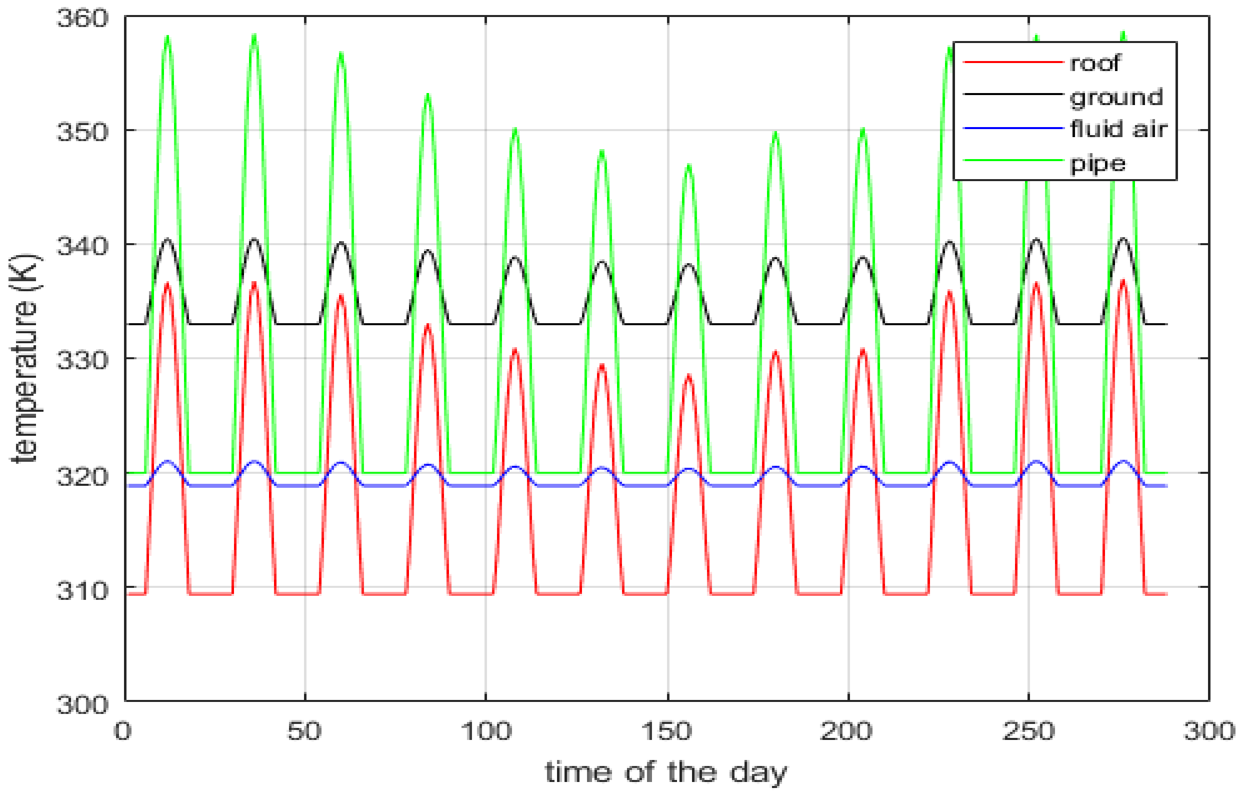

Figure 4. 1 Annually Temperature Variation of Roof, Ground, Fluid Air and Pipe

In Figure 4.3, the daily variations of the representative day of January are plotted. The maximum temperature observed in the time between 10 A.M and 13 P.M for all graphs as shown, which is the maximum solar radiation, occurred. The temperature range of the fluid air is smaller than that of others; this indicates the power output of the plant is nearly constant throughout the day. To show the effect of geothermal water waste heat on the fluid air, Figure 4.2 and Figure 4.3 compared. The increasing recorded temperature is the combined effect of solar radiation and geothermal water waste heat from geothermal power plant.

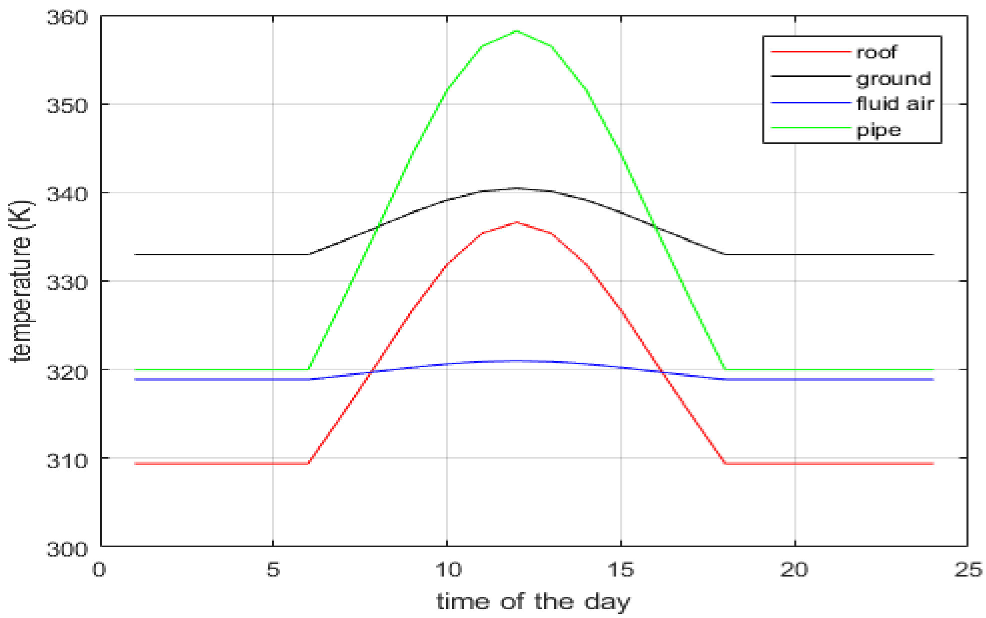

Figure 4. 2 Daily Temperature Variation of Roof, Ground, Fluid Air and Pipe

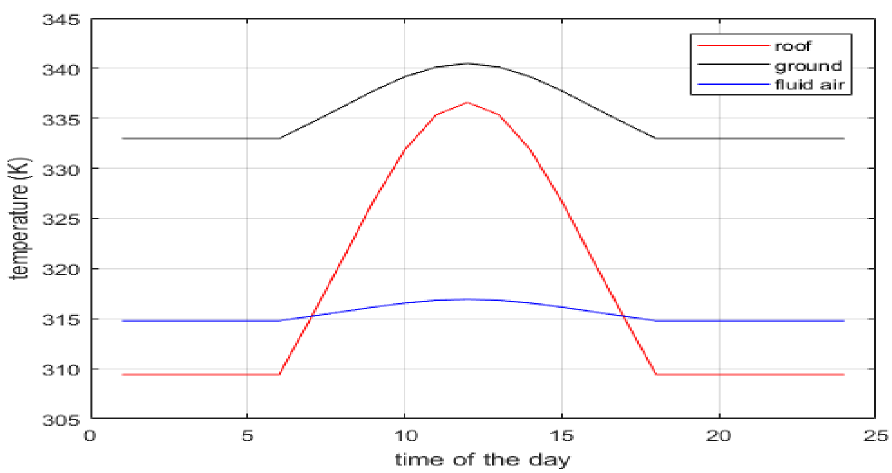

Figure 4. 3 The Output Temperature of Fluid Air without Geothermal Water

Figure 4.4 shows the influence of solar radiation and collector radius on the temperature profile of fluid flowing through the collector. When the solar radiation is constant, the temperature of fluid increases by decreasing the radius and reach maximum at collector outlet. Figure 4.4 imply that, when the solar radiation increases, the air temperature increases for the same collector radius. When the solar radiation increases the collector surface temperature increases and hence the fluid air temperature But as the solar radiation increases above some level, the collector surface temperature increases more and then high convection occurs which results in decrease the mass flow rate of fluid air in the collector.

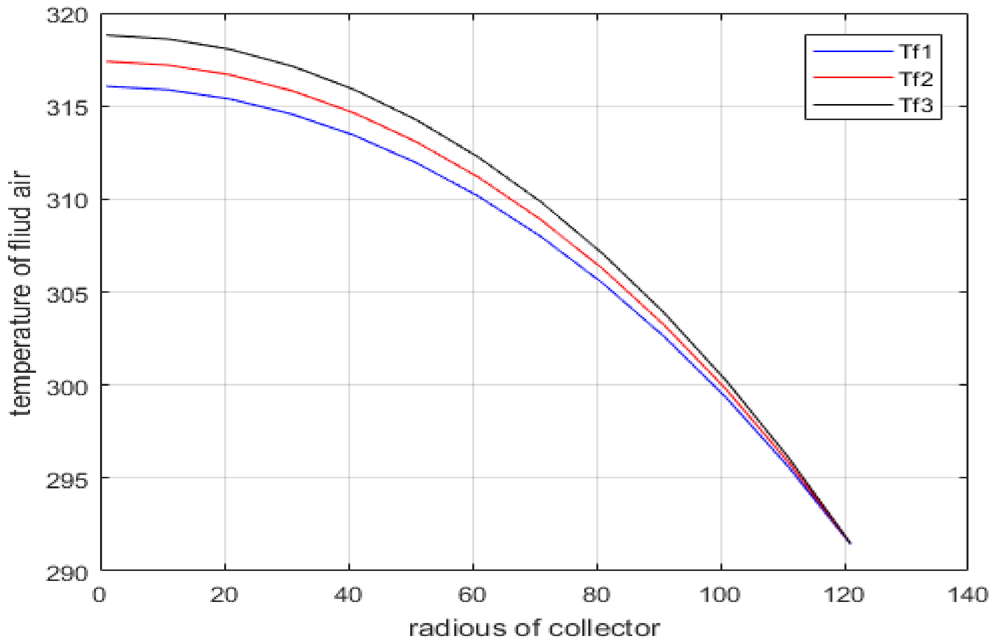

Figure 4. 4 Temperature of Fluid Air at any Radius of Collector

The effect of changing dimensions of the solar chimney power plant on the power generation ranging from 60 to 120 m and chimney height from 50 to 450 m is shown in Figure 4.6 below. These results demonstrate that the larger the collector size and the higher the chimney height is, the greater the power generation will be. it is also evident that the power generation of solar chimney increases nonlinearly with the increase of collector diameter and chimney height. It increases sharply when the sizes of collector and the chimney are small, but slowly with an increase in size . in this study about 123 kW electric power can produced in the solar chimney when the diameter of the collector is 244 m, and the chimney height is 194 m.

Figure 4.5 shows the static pressure profile, which decreases through the collector and drops dramatically near the chimney base. It also demonstrates that increasing solar radiation results in a decrease in the static pressure when the collector radius is constant. Figure 4.7 shows the air velocity profile through the collector. The velocity increases through the collector towards the collector outlet radius, but it increases more sharply by reaching the chimney base. When the collector radius is constant, an increase of solar radiation causes an increase of the air velocity. Examining the effect of collector radius on static temperature and velocity, the trend developing in Figure 4.5 and 4. 7 respectively, have the same effect with the pressure and velocity graphs [60].

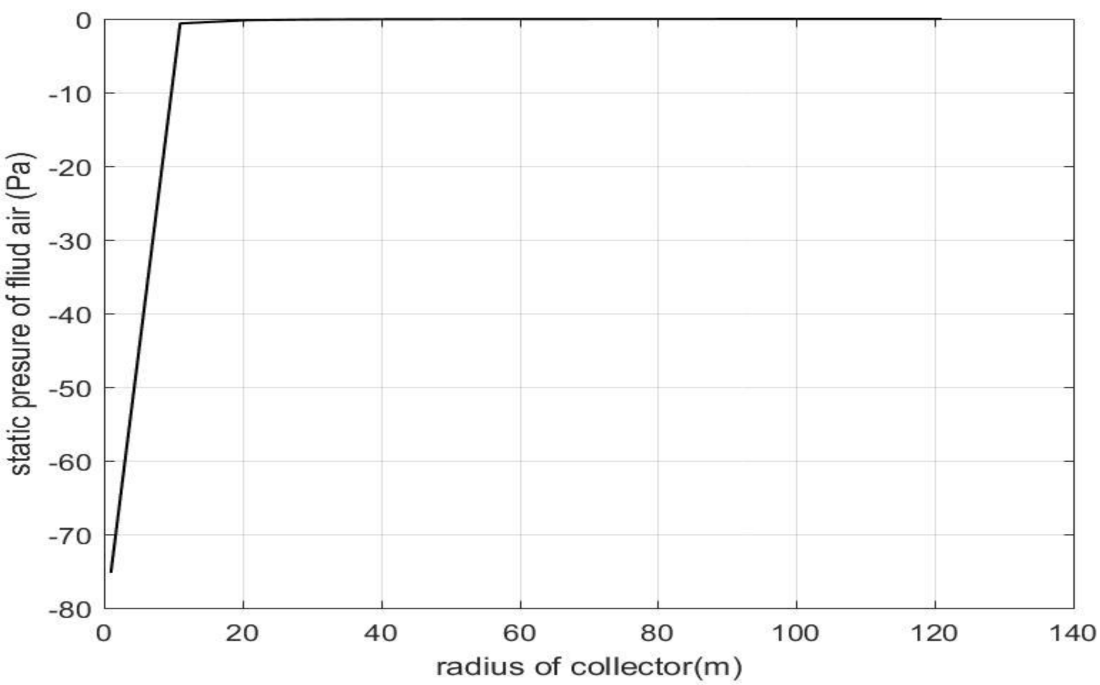

Figure 4. 5 Static Pressure versus Radius of Collector

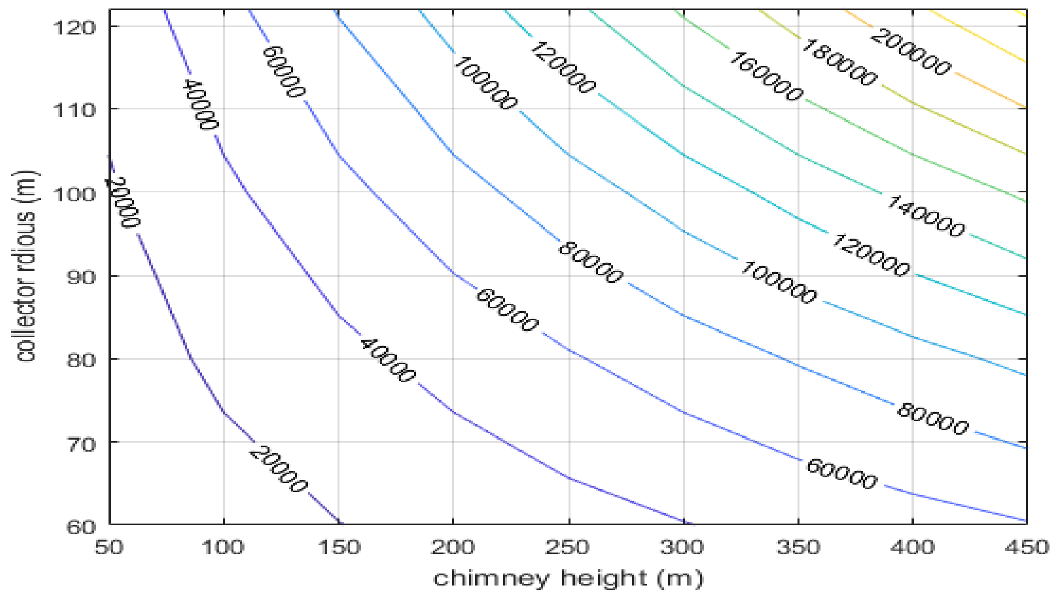

Figure 4. 6 Power Output versus Chimney Height and Collector Radius

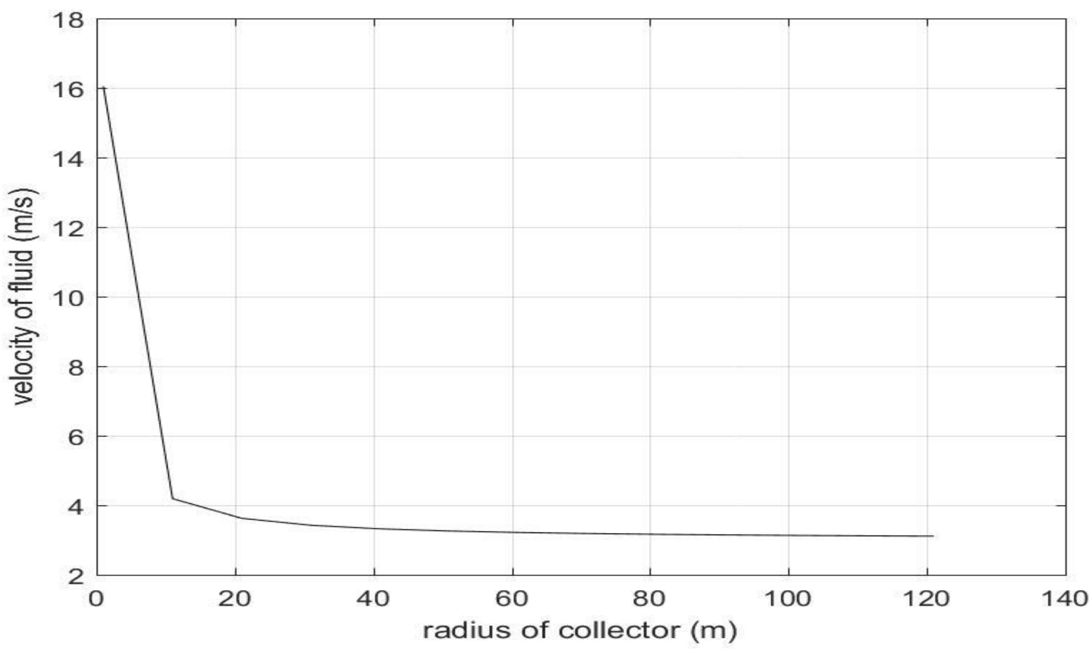

Figure 4. 7 Velocity of Fluid Air versus Radius

In the Table 4.3 the comparison of this, work and previous works done on the reference plant in the literatures. The result of comparison shows there is significance improvement in this work.

Table 4. 3 Comparisons of this Work and Previous Works on Reference Plant

Parameter	**Schalachi, (2005)**	**Asnaghi et al., (2011)**	**Koonsrisuk and Chitsomboon ,(2003)**	**In this work**
V_2(m/s)	15	16.2	15	15.58
T_2(°K)	322		314.5	320.2
ΔT	20	21.8	22	27
Δp_{tur}(Pa)	74	-	-	130.70
Δp_{poten} (Pa)	-	120	135	196.06
p_{load}(kW)	48	265MW/yea	48.3	123.59
η_{coll}	32%	35%	37%	43.58%
η_{ch}	0.65%	0.65%	0.65%	0.653%
η_{tur}	85%	85%	85%	85%
η_{tot}	0.176%	0.1934%	0.204%	0.242%

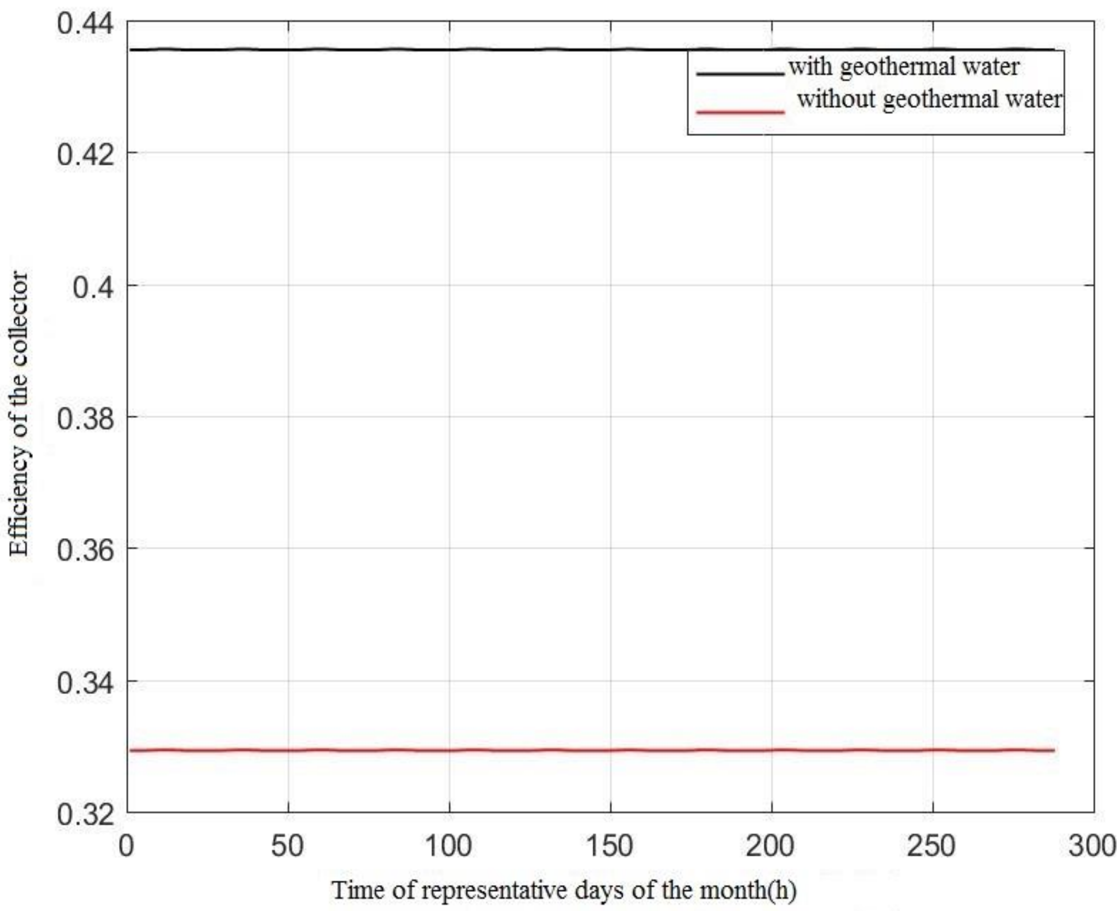

Figure 4. 8 Efficiency of Plant with and Without Geothermal Power Plant

CHAPTER 5
Conclusion and Recommendation

5.1. Conclusion

In this work, the performance analysis of a solar chimney power plant using waste heat from geothermal power plant investigated. The obtained results shows with waste heat of geothermal power plant with mass flow rate 62 kg/s and 90 °C, the collector temperature increases from 316 to 323 K with combined effect of geothermal water and solar radiation as shown in Figure 4.2 and Figure 4.3.

The change in temperature is 27 °C, which is 7 °C increment with Manzanares proto type as shown in Table 4.3. The maximum velocity achieved at the outlet of collector is 15.8 m/s and 182.8 Pa potential pressures observed at the bottom of the chimney. The total pressure drop at the turbine is 120.4 Pa and 62.3 Pa pressure loss occurred due to inlet pressure loss to collector and turbine, the vertical accelerating axial airflow, the inside wall friction, the internal bracing wheel drag forces, and the outlet loss .

The amount of power output increases from 50 kW to 123 kW and efficiency of the collector increases from 32% to 43.58%. Hence, the total efficiency of the solar chimney power plant increased from 0.176% to 0.242%.

The result of the study shows, the solar chimney power plant improved by combining waste heat from another power plant. The model results of this study validated with the previous works and good result has been get with improved efficiency and greater power output.

5.2. Recommendation and Future Work

For future work the following points mentioned;

- Divergent chimney at some angle will enhance the power plant efficiency.
- Transient analysis in time and space for ground, collector roof and geothermal water pipe
- Design of turbine for specific solar chimney can improve the efficiency.
- Considering radial conduction for the ground will improve the efficiency.
- Considering the heat loss along the chimney overestimates the heat loss.

The paper recommend the following point;

- Ethiopia is on the sub-Saharan country there is adequate solar radiation and un populated desert areas .Hence, this work recommend to Ethiopian electric power corporation to work on solar chimney power plant widely.

References

1. REN21 (2017)."Renewables 2017: Global Status Report".
2. BP Statistical Review of World Energy, June, 2016.
3. Teklemariam, M., and Beyene, K., 2000: Geochemical Monitoring of the Aluto Langano Geothermal Field, Ethiopia. Geological Survey of Ethiopia, Addis Ababa, report, 141 pp.
4. Azeb Asnake, Ethiopian Electric Power Corporation reports in london, 2015.
5. Zewdu Woub, Analysis Of Well Test Data From The Langano-Aluto Geothermal Field, Ethiopia ,1998
6. Schlaich J. The solar chimney: Electricity from the Sun. Stuttgart, Germany: Edition Axel Menges; 1995
7. Haaf W, Friedrich K, Mayr G, Schlaich J. Solar Chimneys, Part I: Principle and Construction of the Pilot Plant in Manzanares. Solar Energy 2 (1983)3-20.
8. Haaf W. Solar Towers, Part II: Preliminary Test Results From The Manzanares Pilot Plant, Solar Energy 2 (1984) 141-61.
9. Bernardes MA dos S, Vob A and Weinrebe G. Thermal and Technical Analyses of Solar Chimneys, Solar Energy 75 (2003) 511-24.
10. Ahmed Ayadi, Abdallah Bouabidi, Haytham Nasraoui , Zied Driss and Mohamed Salah Abid, Study of Solar Chimney in Tunisia: Effect of the Chimney Configurations on the Local Flow Characteristics, Energy & Buildings (2018).
11. Xinping Zhou, Yangyang Xu and Fei Zhang, Evaluation of Effect of Diurnal Ambient Temperature Range on Solar Chimney Power Plant Performance, International Journal of Heat and Mass Transfer 115 (2017) 398–405.
12. Tingzhen Ming, Yongjia Wu, Renaud K. de_Richter, Wei Liu and S.A. Sherif, Solar Updraft Power Plant System: A Brief Review and A Case Study on a New System with Radial Partition Walls in Its Collector, Renewable and Sustainable Energy Reviews 69 (2017) 472–487.
13. Shiv Lal, S.C. Kaushik and Ranjana Hans, "Experimental Investigation and CFD Simulation Studies of a Laboratory Scale Solar Chimney for Power Generation”, Sustainable Energy Technologies and Assessments 13 (2016) 13–22.

14. Siyang Hu, Dennis Y.C. Leung and John C.Y. Chan, Impact of the Geometry of Divergent Chimneys on the Power Output of a Solar Chimney Power Plant, Energy 120 (2017) 1-11.
15. Siyang Hu, Dennis Y.C. Leung and John C.Y. Chan, Numerical Modeling and Comparison of the Performance of Diffuser-Type Solar Chimneys for Power Generation, Applied Energy 204 (2017) 948–957.
16. Shachindra Kumar and Dr. Shibayan Sarkar , Numerical Simulation of Solar Updraft Tower, International Journal of Mechanical Engineering (2017).
17. Kamel Milani Shirvan, Soroush Mirzakhanlari, Mojtaba Mamourian and Nidal Abu-Hamdeh, Numerical Investigation and Sensitivity Analysis of Effective Parameters to Obtain Potential Maximum Power Output: A Case Study on Zanjan Prototype Solar Chimney Power Plant, Energy Conversion and Management 136 (2017) 350–360.
18. Fei Cao, Tian Yang, Qingjun Liu, Tianyu Zhu, Huashan Li and Liang Zhao, Design and Simulation of a Solar Double-Chimney Power Plant, Renewable Energy 113 (2017) 764-773.
19. Alibakhsh Kasaeian and Amir Reza Mahmoudi, Fatemeh Razi Astaraei and Afshin Hejab, 3D Simulation of Solar Chimney Power Plant Considering Turbine Blades, Energy Conversion and Management 147 (2017) 55–65.
20. Ahmed Ayadi, Zied Driss, Abdallah Bouabidi and Mohamed Salah Abid, Experimental and Numerical Study of the Impact of the Collector Roof Inclination on the Performance of a Solar Chimney Power Plant, Energy and Buildings 139 (2017) 263–276.
21. Ahmed Ayadi, Zied Driss, Abdallah Bouabidi,Haithem Nasraoui, Moubarek bsisa and Mohamed Salah Abid, A Computational and an Experimental Study on the Effect of the Chimney Height on the Thermal Characteristics of a Solar Chimney Power Plant, j.Process Mechanical Engineering (2017)1-14.
22. Arkan k. Al-Taaie, Waheeds S. Mohammad, Abbas J. Jubear, Numerical Simulation of the Collector Angle Effect on the Performance of the Solar Chimney Power Plant, Al-Khwarizmi Engineering Journal,Vol. 12, No. 2, P.P. 79- 89 (2016).

23. Aakash Hassan, Majid Ali and Adeel Waqas, Numerical Investigation on Performance of Solar Chimney Power Plant by Varying Collector Slope and Chimney Diverging Angle, Energy 142 (2018) 411-425.
24. Young Jae Choi, Dong Hoon Kam, Yoon Won Park and Yong Hoon Jeong, Development of Analytical Model for Solar Chimney Power Plant with and without Water Storage System, Energy 112 (2016) 200-207.
25. Mostafa A.H. Abdelmohimen and Salem A. Algarni, Numerical Investigation of Solar Chimney Power Plants Performance for Saudi Arabia Weather Conditions, Sustainable Cities and Society 38 (2018) 1–8.
26. Omer Khalil Ahmed and Abdullah Sabah Hussein, New Design of Solar Chimney (Case Study), Case Studies in Thermal Engineering 11 (2018) 105–112.
27. Nima Fathi, Patrick McDaniel, Seyed Sobhan Aleyasin, Matthew Robinson, Peter Vorobieff, Sal Rodriguez and Cassiano de Oliveira, Efficiency Enhancement of Solar Chimney Power Plant by Use of Waste Heat from Nuclear Power Plant, Journal of Cleaner Production 180 (2018) 407-416.
28. Fei Cao, Qingjun Liu, Tian Yang, Tianyu Zhu, Jianbo Bai and Liang Zhao, Full-Year Simulation of Solar Chimney Power Plants in Northwest China, Renewable Energy 119 (2018) 421-428.
29. Tahar Tayebi and Mahfoud Djezzar, Effect Of Varying Ambient Temperature and Solar Radiation on the Flow in a Solar Chimney Collector, International Journal of Smart Grid and Clean Energy, vol. 5 , no. 1, January 2016.
30. Penghua Guo, Jingyin Li, Yunfeng Wang and Yuan Wang, Evaluation of the Optimal Turbine Pressure Drop Ratio for A Solar Chimney Power Plant, Energy Conversion and Management 108 (2016) 14–22.
31. Parishwang Piyush and Ankur Pandey, Analysis (Data) of Chimney Operated Solar Power Plant, International Journal Of Innovative Research In Science, Engineering and Technology, Vol. 5, Issue 3, March 2016.
32. Jianlan Li, Hongjing Guo and Shuhong Huang, Power Generation Quality Analysis and Geometric Optimization for Solar Chimney Power Plants, Solar Energy 139 (2016) 228–237.

33. Mehrdad Ghalamchia, Alibakhsh Kasaeian, Mehran Ghalamchi and Alireza Hajiseyed Mirzahosseini, Experimental Study on the Thermal Performance of a Solar Chimney with Different Dimensional Parameters, Renewable Energy 91 (2016) 477-483.
34. Nima Fathi, Patrick McDaniel, Seyed Sobhan Aleyasin, Matthew Robinson, Peter Vorobieff, Sal Rodriguez and Cassiano de Oliveira, Efficiency Enhancement of Solar Chimney Power Plant by Use of Waste Heat From Nuclear Power Plant, Journal of Cleaner Production 180 (2018) 407-416.
35. Filip V. Stojkovski, Marija Chekerovska, Risto V. Filkoski and Valentino Stojkovski, Numerical Modeling of A Solar Chimney Power Plant, International Journal of Contemporary energy, Vol. 2, No. 1 (2016).
36. Mehdi Mehrpooyaa, Mohsen Shahsavan , Mohammad Mehdi and Moftakhari Sharifzadeh, Modeling Energy and Exergy Analysis of Solar Chimney Power Plant-Tehran Climate Data Case Study, Energy 115 (2016) 257-273.
37. Mehran Ghalamchia, Alibakhsh Kasaeian and Mehrdad Ghalamchi, Experimental Study of Geometrical and Climate Effects on the Performance of a Small Solar Chimney, Renewable and Sustainable Energy Reviews 43 (2015) 425–431.
38. Penghua Guo, Jingyin Li, Yunfeng Wang and Yuan Wang, Evaluation of the Optimal Turbine Pressure Drop Ratio for A Solar Chimney Power Plant, Energy Conversion and Management 108 (2016) 14–22.
39. Penghua Guo, Jingyin Li, Yunfeng Wang, Yuan Wang, Numerical Study on the Performance of a Solar Chimney Power Plant, Energy Conversion and Management 105 (2015) 197–205.
40. Atit Koonsrisuk and Tawit Chitsomboon, Mathematical Modeling of Solar Chimney Power Plants, Energy 51 (2013) 314-322.
41. Ehsan Shabahang Nia and M. Ghazikhani, Numerical Investigation on Heat Transfer Characteristics Amelioration of A Solar Chimney Power Plant through Passive Flow Control Approach, Conversion and Management 105 (2015) 588–595.
42. Babak Ghorbani, Mohammad Ghashami, Mehdi Ashjaee and Hamid Hosseinzadegan, Electricity Production with Low Grade Heat in Thermal Power Plants by Design Improvement of a Hybrid Dry Cooling Tower and a Solar Chimney Concept, Energy Conversion and Management 94 (2015) 1–11.

43. Sandeep K. Patel, Deepak Prasad and M. Rafiuddin Ahmed, Computational Studies on the Effect of Geometric Parameters on the Performance of a Solar Chimney Power Plant, Energy Conversion and Management 77 (2014) 424–431.
44. Arkan khilkhal Husain , Waheeds Shate Mohammad and Abbas JassimJubear, Numerical Simulation of the Influence of Geometric Parameter on the Flow Behavior In a Solar Chimney Power Plant System, Journal of Engineering, Number 8 Volume 20 (2014) .
45. Kai Chen, Jiangfeng Wang , Yiping Dai and Yuqi Liu, Thermodynamic Analysis Of A Low-Temperature Waste Heat Recovery System Based on the Concept Of Solar Chimney, Energy Conversion and Management 80 (2014) 78–86.
46. Babkir Ali, Techno-Economic Optimization for the Design of Solar Chimney Power Plants, Energy Conversion and Management 138 (2017) 461–473.
47. Mohammed H. Ali, Analysis Study of Solar Tower Power Plant & Its Configuration Effects on Its Performance in Iraq (Baghdad City) ,Vol. 7, No. 4; 2013 .
48. Mohammad O. Hamdan, Analysis of Solar Chimney Power Plant Utilizing Chimney Discrete Model, Renewable Energy 56 (2013) 50-54.
49. Xinping Zhou and Yangyang Xu, Solar Updraft Tower Power Generation, Solar Energy 128 (2016) 95–125.
50. Ehsan Gholamalizadeh and Man-Hoe Kim, CFD (Computational Fluid Dynamics) Analysis of a Solar Chimney Power Plant with Inclined Collector Roof, Energy 107 (2016), 661-667.
51. Salah Larbi, Amor Bouhdjar and Toufik Chergui, Performance Analysis of a Solar Chimney Power Plant in the Southwestern Region of Algeria, Renewable and Sustainable Energy Reviews, 14 (2010) 470–477.
52. Xinping Zhou, Shuo Yuan, Marco Aurelio dos Santos Bernardes, Sloped-Collector Solar Updraft Tower Power Plant Performance, International Journal of Heat and Mass Transfer 66 (2013) 798–807.
53. Bilgen E, Rheault J. Solar Chimney Power Plants for High Latitudes. Solar Energy 2005; 79:449.

54. Pasumarthi N, Sherif SA. Experimental and Theoretical Performance of a Demonstration Solar Chimney Model, Part I: Mathematical Model Development. International journal of Energy Research , 22, 443-461 (1998).
55. Duffie, J.A., Beckman, W.A. Solar Engineering of Thermal Processes, Wiley Inter. science, New York. 1991, fourth edition
56. Yunus A.cengel, Heat Transfer, second edition.
57. Pretorius JP, Kroger DG. Solar Chimney Power Plant Performance. ASME J SolarEnergy Eng 2006;128:302
58. D. Sharp, Wind Power 1 and 2, Wind Turbine Aerodynamics, Loughborough University.
59. A. Asnaghi, S.M. Ladjevardi, Solar chimney power plant performance in Iran, Renewable and Sustainable Energy Reviews 16 (2012) 3383– 3390.
60. Roozbeh Sangi, Majid Amidpour and Behzad Hosseinizadeh, Modeling and Numerical Simulation of Solar Chimney Power Plants, Solar Energy 85 (2011) 829–838.
61. Pope, Stephen. "Turbulent Flows". Cambridg University Press, 2000.
62. Gannon, A.J., Von Backström, T.W., (Aug 2000), Solar Chimney Cycle Analysis with System Loss and Solar Collector Performance, ASME Journal of Solar Energy Engineering, Vol. 122, no. 3, pp 133-137.

APPENDIX: 1 MATLAB Code to Find Temperature Variation

```
clear all
clc
```

Parameters for solar chimney dimensions

```
hch=124;      % height of chimney in meter
dch=11.06;    % dimeter of chimney in meter
hcol11=1.85;  % height of collector at inlet
hcoll2=66;    % height of collector at outlet
beta=30;      % inclination of collcetor
```

Geothermal water properties at70 0c

```
mw=62.5;        % mass flow rate of water in kg/s
cpw=4190;       % specific heat of water j/kg.k
rhow=977.5;     % density of geothermal water kg/m^3
kw=0.663;       % thermal conductivity of water W/m.K
prw=2.55;
muew=1.126*10^(-5);
```

```
%%%% fluid air properties at mean temperature( 18+45)/2=31.5
mf=1525;                % mass flow rates of fluid air
cpf=1007;               % specific heat of fluidj/kg.k
rhof=1.1564;            % density of fluid air
muef=1.8812*10^(-5);    % dynamic viscousity
v=1.6268*10^(-5);       % kinamatic viscousity
prf=0.7276;
kf=0.0260;
```

Roof properties

```
cpr=903;       % specific heat of roof
trar=0.8;      %transmitivity of roof
kr=273;        %thermal conductivity of aluminium roof
rhor=2702;     %density of roof aluminium
```

```
emr=0.09;       % emisivity of roof
absor=0.26;     %absorpitivity of roof
lr=0.025;       % thickness of roof
r=122;          % dimeter of collcctor at inlet
dr=122;         % section of collector
s=132;          %inclined length of roof
Ar=0.5*3.14*r*s;    %area of collector roof
%
```

Ground properties (treated soil)

```
cpg=710;        % specific heat of absorber
rhog=2160;      %density ofabsorber.................
absog=0.9;      %absorpitivity of absorber
emg=0.9;        % emisivity of asorber
kg=1.83;        % thermal conductivity of absorber
zg=0.5;         %thickness of ground
pi=3.14;
Ag=pi*r*dr;
```

```
%pipe properties stainless steel
Dp=0.208;       %diameter of pipe
zp=0.004;       %pipe thickness
lp=15335;       %length of pipe
Ap=pi*Dp*lp;    %area of pipe
trap=0.5;       %transmitivity of pipe
rhop=8055;      %kg/m3 density of pipe carbon steel
cpp=456;        % specific heat of pipe j/kg.k
kp=15.1;        %thermal conductivity of pipe
absop=0.11;     %absorpitivity of pipe
emp=0.18;       % emissivity of pipe
pi=3.14;
sigma=5.06*10^(-8);% stefan boltzman constant w/m^2.k^4
```

```
%%%boundary conditions
Ta=291;               % initial ambient temperature
Tf1=293;              % inlet fluid temperature
Tsky=Ta-6;            % sky temperature
Tw1=363;              % inlet geothermal water temperature in degree celicius
```

```
Tw2=Ta+20;            % exit tempreature of water
Twm=0.5*(Tw1+Tw2);    %mean water temperature
```

```
%%assumed input conditions
Tf2=318;           % initial exit temprature of fluid
Tfm=(Tf1+Tf2)/2;   % meanfliud temperature
Tr=300;            % initial roof temprature
 Tp=330;           % initial temperature of pipe
Tg=333;            %assumed initial temperature of absorber
```

```
%air properties from the table at 300k----------------------
cpa=1007;             %heat capacity of air J/kg.k
Ka=0.0257;            %thermal conductivity of air w/m.k
muea=1.81e-5;         % dynamic viscosity of air kg/m.s
va=1.52e-5;           % kinematic viscosity of air m^2/s
rhoa=1.184;           %density of air [kg/m^3]
g=9.81;               %gravity
uf=3;                 %velocity of wind
```

```
%convection coefficient for ground to fluid air at mean temperature
prgf=0.738;          %prandtel number
cpgf=1007;           %specific heat capacity
rhogf=1.1076;        %density
kgf=0.0271;          %thermal conductivity
lcgf=122;            %critical length
Tgf=333;             %temperature of ground
Tfm=305.5;           %mean fluid temperature
B=1/Tfm;             %temperature expansion
g=9.81;              %gravity
muegf=1.3479*10^(-5);%dynamic viscousity
vgf=1.759*10^(-5);   %kinamatic viscousity
f=0.0336;            %friction factor
uf=9;                %velocity of fluid
Gr=g*B*(Tgf-Tfm)*(lcgf^3)/vgf^2;
Regf=rhogf*uf*lcgf/muegf;
Ra=Gr*prgf;
hcgf=3.5;%((f/8)*(Regf-1000)*prgf*(kgf/lcgf))/(1+12.7*((f/8)^0.5)*(prgf^(2/3)-1));
```

Convection coefficient for circular pipe to fluid air at mean temperature

```
g=9.81;           %gravity
Tpf=338;           % mean temperature of pipe
Tfmf=322;          %mean temperature of fluid
B=1/Tfm;
cppf=1007;
vpf=1.788*10^(-5);
muepf=.9586*10^(-5);%
kpf=0.0273;
lcpf=0.208;% is equal to out side diameter of pipe
prpf=0.7231;
rhopf=1.0954;
Repf=rhopf*uf*lcpf/muepf;
Nupf=0.027*Repf^0.805*prpf^0.3333;
hcpf=(kpf/lcpf)*Nupf;
```

Convection roof to fluid air

```
krf=0.0267;
rhorf=1.1234;
prrf=0.7252;
Tfm=314;
Tr=323;
f=0.0336;
betha=30;
B=1/Tfm;
lcrf=122;
muerf=1.9730*10^(-5);
vrf=1.7116*10^(-5);
uf=9;
Rerf=rhorf*uf*lcrf/muerf;
Ra=(9.81*0.866*B*(Tr-Tfm)*lcrf^3*prrf)/(vrf^2);
Nurf=(0.825+(0.387*(prrf^0.5)*Ra^0.16667)/(1+(0.0492/prrf)^0.5625)^0.29629)^2;
hcrf=3;%((f/8)*(Rerf-1000)*prrf*(krf/lcrf))/(1+12.7*((f/8)^0.5)*(prrf^(2/3)-1));
```

Convection coefficient for collector roof to ambient at mean temperature of

```
uw=3;              % velocity of wind
rhora=1.1488;        % density of fluid air
```

```
cpra=1007;           % specific capacity offluid air
prra=0.7271;         % prandtel number
hcra=3.87+0.0022*(uw*rhora*cpra)/prra^(2/3);
```

```
%%%%  radiation coefficients
hrrsky=sigma*emr*(Tr^2+Tsky^2)*(Tr+Tsky);      %between roof and sky
hrpr=sigma*(Tp^2+Tr^2)*(Tr+Tp)/(1/emp+1/emr-1); %between roof and pipe
hrrp=hrpr;
hrgr=sigma*(Tg^2+Tr^2)*(Tg+Tr)/(1/emg+1/emr-1); %between ground and roof
hrrg=hrgr;
hrpg=sigma*(Tp^2+Tg^2)*(Tp+Tg)/(1/emp+1/emg-1); %between pipe and ground
hrgp=hrpg;
```

Radiation data

```
phi=7.78;           % latitude of aluto langano
dt=3600;
for i=1          %time step of the collected radiation
```

```
load tot.m          %the monthly average hourly global and diffuse radiation
data1=zeros(24,1);
```

```
for j=1:12
   data1(:,:,j)=tot(j+(23*(j-1)):j*24,:);
end
 i=1:288;
   IT=data1(i);

 Ir=IT(i)*absor;
 I=transpose(Ir);
 Ip=IT(i)*absop*trar;
 Ig=IT(i)*absog*trap;
%  temperature of the roof ,fluid and ground

  Tr1i=Tr-(dt/(cpr*rhor*pi*r*s*lr))*Tr*(Ar*hcra+Ar*hcrf+Ap*hrpr+Ar*hrrsky+Ag*hrgr)+...

(dt/(cpr*rhor*pi*r*s*lr))*(Ar*Ir+Ap*hrpr*Tp+Ar*hcrf*Tfm+Ar*hcra*Ta+Ar*hrrsky*Tsky+Ag
*hrgr*Tg);

 Tpi=Tp-
```

```
(dt/(cpp*rhop*pi*Dp*zp*lp))*Tp*(Ar*hrrp+Ag*hrgp+2*3.14*0.104*lp/(log(0.208/0.204))+0.5*
Ap*hcpf)+...

(dt/(cpp*rhop*pi*Dp*zp*lp))*(0.5*Ap*Ip+Ar*hrrp*Tr+Ag*hrgp*Tg+2*3.14*0.104*lp/(log(0.2
08/0.204))*Twm+0.5*Ap*hcpf*Tfm);



 Tgi=Tg-(dt/(cpg*rhog*pi*r*dr*zg))*Tg*(Ar*hrrg+Ap*hrpg+Ag*hcgf)+...
    (dt/(cpg*rhog*pi*r*dr*zg))*(Ar*hrrg*Tr+Ap*hrpg*Tp+Ag*hcgf*Tg+Ag*Ig);

Tf2i=Tf2*(1-1/dr)+((1/(mf*cpf))*(Ar*hcrf*(Tr1i-Tfm)+Ap*hcpf*(Tp-Tfm)+Ag*hcgf*(Tgi-
Tfm)-((mf*cpf*Tf1)/dr)));
```

```
     end
```

```
%this stores  plots on january month
 y=1:288;
% to plot on the same plane
 plot(y,Tr1i,'-r')
 hold on
plot(y,Tgi,'-black')
hold on
 plot(y,Tf2i,'-blue')
hold on
plot(y,Tpi,'-green')
grid on
  hold off
 legend('roof','ground','fluid air','pipe')
xlabel('time of the day')
ylabel('temperature (K)')
```

Published with MATLAB® R2017a

APPENDIX: 2 MATLAB Code to Calculate Power Output and Efficiency

```
clear all
clc
T1=291;heff=194.6;hsut=167.7937;hcoll=26.8063;Dsut=10.16;pi=3.14;
Ar=5.5450e4;Asut=81.03;A2=Asut;A1=1417.39;
R=287;cp=1005;rr=122.2;rc=5.08;x=0.66667;f=0.008428;
a=0.65;U=15;g=9.81;
pinf1=101325;Tinf1=293;
rhoinf1=pinf1/(Tinf1*R);
rho1=rhoinf1;cpw=4190;mw=62.5;
v1=0.8;T3=319;%guss
 v1c=3;T3c=320;
 load useful.m          %useful heat gain
data1=zeros(24,1);
```

```
for j=1:12
    data1(:,:,j)=useful(j+(23*(j-1)):j*24,:);
end
  i=1:288;
     qu=1.0e+6*data1(i);%useful heat gain
 while (v1c-v1)/v1>0.015&(T3c-T3)/T3<0.034
 v1=v1c;
       T3=T3c;
p1=pinf1-0.5*rho1*v1^2;
T1=293;%inlet  temperature of fluid air
rho1=p1/(T1*R);%inlet density of fluid air
m=1400;%mass flow rate of fluid  air
T2=318;%temperature of fluid air at outlet of collector
p2=p1+((m*qu)./(2*3.14*hcoll^2*rho1*cp*T1))*(log(rr/rc))-(m^2/(2*rho1))*(1/A2^2-
1/A1^2);%pressure of fluid air at outlet of collector
rho2=p2./(T2*R);%density of fluid air at outlet of collector and inlet of chimney
dt=T2-T1;%change in temperature inthe collector
v2=m./(rho2.*A2);%velocity at outlet of collector and inlet if chimney
p4=pinf1*(1-(g*heff/(cp*Tinf1)))^3.5;%pressure at outlet of turbine
ppoten=pinf1*(1-((1-g*heff/(cp*Tinf1))/(1-g*hsut/(cp*T3)))^3.5)-
((g*hcoll*pinf1)/(2*R*Tinf1))*(1+(Tinf1/T3)*((1-g*heff/(cp*Tinf1))/(1-g*hsut/(cp*T3)))^3.5);
ptur=ppoten.*x;%pressure drop on the turbine
```

```
pturi=0.14*0.5*rho2.*v2.^2;%pressure loss at inlet of turbine
 p3=p2-pturi-ptur;%pressure after turbine
ploss=ppoten-ptur;%pressure loss through the wole system
rho3=p3/(T3*R);I=235;%densityof fluid air after turbine
T4=T3-(g*heff/cp);%temperature at outlet of chimney
 rho4=p4/(T4*R);%density of fluid air at outlet of chimney
v3=(ploss./((((0.14*rho3/rho2)+0.25+(0.008428*hsut/Dsut))*0.5*rho3)+0.5*1.26*rho4)).^0.5;%
calculated velocity at outlet of turbine
rhoavg=(p2+p3)/(R*(T3+T2));%average density of fluid air in the collector
vavg=m./(Asut*rhoavg); %average vlocity of fluid air in the collector
T3c=T2-(Asut.*ptur.*vavg)./(cp.*m);%calculated temperature at outlet of turbine
v1c=(rho3.*v3*Asut)./(rho1*A1);%calculated  collector inlet velocity of fluid air
 power=0.8*ptur*Asut.*vavg;%electrical power output

 end
effcoll=qu./((I.*Ar)+mw*cpw*(90-38));%efficiency of the collector
  chimeff=g*heff/(cp*T1);%chimney efficiency
  toteff=effcoll*0.85*chimeff;% total efficiency of the system
```

Published with MATLAB® R2017a

APPENDIX: 3 MATLAB Code to Plot Variation of Velocity, Temperature and Pressure with Collector Radius

```
clear all
clc
mf=1525;cpf=1007;Tc1=298;Tc2=303;Tc3=308;Ta=291;Tg1=329;Tg2=333;
Tg3=338;Tp1=310;Tp2=320;Tp3=330;ri=1:10:122;cp=1007;
h=2.8;%heat transfer coefficient
```

```
m=2*3.14*h*(ri.^2-122^2)/(cpf*mf);
Tf1=0.5*(Tc1+Tg1+Tp1+(2*Ta-Tc1-Tg1-Tp1).*exp(m));%temperature of fluid air with respect
to radius
Tf2=0.5*(Tc2+Tg2+Tp2+(2*Ta-Tc2-Tg2-Tp2).*exp(m));
Tf3=0.5*(Tc3+Tg3+Tp3+(2*Ta-Tc3-Tg3-Tp3).*exp(m));
```

```
da=1.1564;%density of air
r=122;
 ri=1:10:122;
df=2.829-0.0084.*Tf1+0.00001.*Tf1.^2-5*10^(-9).*Tf1.^3;
uf=mf./(2*3.14*ri*11.55.*df);%velocity of fluid air
p1=mf^2.*da.*(1/r^2-1./ri.^2)./(8*1.85^2*3.14^2.*df.^2);%pressure at any radius
```

```
p=p1(1:13)
plot(ri,p,'black')
grid on
xlabel('radius of collector')
ylabel('presure of fliud air')
```

```
plot(ri,Tf1,'-blue')
hold on
plot(ri,Tf2,'-red')
hold on
plot(ri,Tf3,'black')
grid on
hold off
legend('Tf1','Tf2','Tf3')
xlabel('radius of collector')
ylabel('temperature of fliud air')
```

```
u=uf(1:13)
plot(ri,uf,'-black')
grid on
xlabel('radius of collector')
ylabel('velocity of fluid')
```

Published with MATLAB® R2017a

APPENDIX: 4 Material Properties Used In the Calculation

Material types	Properties of material	value
Cover material properties	Cover material	Aluminum
	Cover emissivity	0.095
	Absorber Absorptivity	0.09
	Transmissivity	0.8
	Thickness (m)	0.0025
	Density (kg/m^3)	2702
	Thermal conductivity (W/m.K)	273
	Specific heat capacity (J/kg.K)	903
Ground [bernards et al 2010]	type	Sandstone
	Absorptivity (treated surface)	0.9
	Emissivity (treated surface)	0.9
	Thickness (m)	0.5
	Thermal conductivity (W/m.K)	1.83
	Specific heat capacity	710
	Density (kg/m^3)	2160
Geothermal water pipe	Material	stainless steel AISI 302
	Absorptivity	0.41
	Emissivity	0.17
	Transmissivity	0.5
	Internal Diameter (m)	0.204
	Thickness (m)	0.004
	Length (m)	15472
	Thermal conductivity(W/m.K)	15.1
	Specific heat capacity (J/kg.K)	456
	Density (kg/m^3)	8055
Geothermal water	Specific heat capacity (J/kg.K)	4190
	Density(kg/m^3)	977.5
	Thermal conductivity(W/m.K)	0.663
Location	Aluto langano Latitude	7.78
	Aluto langano Longitude	38.79
	Ambient maximum and minimum temperature	18 °C, 25 °C